Journal of Molecular Liquids 393 (2024) 123569

Contents lists available at ScienceDirect

Journal of Molecular Liquids

journal homepage: www.elsevier.com/locate/molliq

Exploration the effect of selenophene moiety and benzothiophene based acceptors on optical nonlinearity of D–π–A based heterocyclic organic compounds in chloroform solvent: A DFT approach

Iqra Shafiq [a,b,1], Muhammad Khalid [a,b,*,1], Ataualpa A.C. Braga [c], Zara Tariq [a,b], Norah Alhokbany [d], Ke Chen [e,*]

[a] Institute of Chemistry, Khwaja Fareed University of Engineering & Information Technology, Rahim Yar Khan, 64200, Pakistan
[b] Centre for Theoretical and Computational Research, Khwaja Fareed University of Engineering & Information Technology, Rahim Yar Khan, 64200, Pakistan
[c] Departamento de Qúmica Fundamental, Instituto de Qíumica, Universidade de Saõ Paulo, Av. Prof. Lineu Prestes, 748, Sao Paulo, 05508-000, Brazil
[d] Department of Chemistry, King Saud University, Riyadh 11451, Saudi Arabia
[e] Department of Infectious Diseases, The Affiliated Hospital of Southwest Medical University, Luzhou 646000, China

ARTICLE INFO

Keywords:
Fullerene free
Structure modeling
Hyperpolarizability
DFT study
FMOs

ABSTRACT

Currently, fullerene-free organic chromophores find widespread use in the endeavor to enhance the efficacy of NLO materials. Considering the significance of NF organic systems, we fabricated a push-pull series of heterocyclic organic compounds (**DTPD1-DTPD8**) from **DTPR** by molecular engineering with benzothiophene acceptors at one terminal. Owing to the larger size, greater charge transference and higher polarizability nature of selenophene than that of thiophene, the π-spacer was replaced with selenophene. The effect of selenophene moiety and benzothiophene based acceptors on optical nonlinearity of **DTPD1-DTPD8** was explored through quantum chemical study. DFT approach at M06/6-311G(d,p) functional was employed in order to explore the optoelectronic properties of designed chromophores. The FMOs findings disclosed a substantial reduction in band gaps (2.107–3.057 *eV*) in derivatives than that of **DTPR** (3.12 *eV*). An effective charge transference from donor to acceptor *via* spacer was observed in HOMO/LUMO which further supported by DOS and TDM heat maps. GRPs findings revealed that all derivatives had higher softness ($\sigma = 0.327–0.475\ eV^{-1}$) with lower hardness ($\eta = 1.04–1.53\ eV$) than that of **DTPR** which expressed the higher polarization in derivatives. Significant advancements in nonlinear optical (NLO) outcomes were obtained for all the derivatives as compared to reference chromophore. Particularly, **DTPD6** exhibited the efficient response [$<\alpha> = 1.561\times10^{-22}$, $\beta_{total} = 2.111\times10^{-27}$ *esu*] among all tailored chromophores owing to its unique characteristics such as reduced band gap (2.107 *eV*) highest softness value (0.475 *eV*) with lowest hardness value at 1.04 *eV*. This structural modification by utilizing selenophene π-spacer and benzothiophene acceptor played a protruding role in attaining promising NLO responses. Thus, this study tempted the experimentalists to synthesize the proposed NLO materials for the modern optoelectronic high-tech applications.

1. Introduction

Non-linear optical (NLO) materials are emerging as a cornerstone in the evolution of information materials, owing to their unique information processing attributes and ultra-swift responsiveness, thereby significantly extending the laser's spectral range [1-5]. NLO materials have a broad range of applications, encompassing fields such as, biological imaging, lasers, photoelectric switches, spectrum analysis, environmental monitoring and various other scientific disciplines [6-9]. The search for innovative NLO compounds has historically relied on chemical synthesis, prompting extensive research endeavors aimed at creating more efficient materials. Presently, quantum chemistry has advanced to a level where its theoretical accuracy can substantially contribute to predicting the performance of newly designed NLO compounds and the enhancements achievable through chemical modifications or controlled strategies for traditional materials [10-12]. The

* Corresponding authors.
E-mail addresses: Khalid@iq.usp.br (M. Khalid), chitty8705@sina.com (K. Chen).
[1] Both authors contributed equally

https://doi.org/10.1016/j.molliq.2023.123569
Received 17 October 2023; Received in revised form 8 November 2023; Accepted 10 November 2023
Available online 11 November 2023

evolution of society and the increasing demand for communication are acting as catalysts for advancing the research and development of NLO materials [13]. Optoelectronic [14] systems have predominantly employed inorganic crystals as their nonlinear optical (NLO) counterparts. Ongoing scientific endeavors are focused on the exploration of novel crystals [15-17] with enhanced NLO properties [18].

In recent decades, extensive research efforts have been dedicated to investigating bulk materials which possess efficient NLO characteristics. This exploration encompasses a wide range of materials, including organometallic [19], inorganic [20], organic–inorganic hybrids [20,21] and purely organic materials [22]. Each category of material possesses distinctive characteristics, but organic NLO substances have demonstrated superior efficacy in contemporary solar cell applications. This is primarily attributed to their exceptional flexibility and low relative permittivity, facilitating robust modifications. Additionally, they are deemed efficient NLO materials owing to their capacity to withstand high damage thresholds, cost-effectiveness and reasonably high photoelectric coefficients [23,24]. Among the various categories of NLO materials, fullerene acceptor molecules exhibit substantial nonlinear properties [25]. However, fullerene-based compounds have certain disadvantages, including their restricted photostability and reduced ability to absorb light in the visible spectrum [26,27]. Recently, non-fullerene compounds have gained prominence in NLO materials. They offer cost-effectiveness, strong light absorption, versatility in synthesis and low toxicity [28].

Researchers commonly employ a fundamental design strategy involving the incorporation of robust donor (D) and acceptor (A) groups at opposite ends of a π-conjugated bridge. This configuration leads to development of high degree of polarizable molecules, which exhibit substantial NLO properties. In the previous twenty years, researchers have explored various π-conjugated bridges to assess their impact not only on NLO response but also on factors like photochemical durability, thermal stability and solubility [29,30].The scientific literature describes a range of structural configurations, including D-A, D-π-A, D-π-A-π-D, A-π-D-π-A, D-π-π-A, D-A-π-A, and D-D-π-A [31,32]. Moreover, investigations based on both experimental and theoretical outcomes have revealed that the incorporation of potent donor (D), acceptor (A) and π-spacer groups can enhance NLO response [33]. This is called push-pull system. The HOMO–LUMO band gap, closely tied to the push–pull mechanism [34], narrows when a system comprises highly electronegative groups connected to electron-rich groups through π-spacers. This reduction in E_{gap} directly influences intramolecular charge transfer (ICT), enhancing the potential for designing superior NLO compounds [35].

The enhancement of NLO responses in compounds demonstrating substantial charge transfer can be achieved by extending the conjugation length and reinforcing the potency of donor/acceptor groups [36]. However, the expansion of the π -conjugated system and the intensification of electron-donor and electron-acceptor groups lead to a bathochromic shift. Furthermore, multiple research groups have documented the π-spacer segments, which consist of selenophenes, thiophenes, and benzothiadiazides [37]. According to literature sources, the decreased aromaticity of selenophene in comparison to thiophene contributes to a reduced band-gap energy, an increased effective conjugation length, and improved planarity. Additionally, materials based on selenophene exhibit enhanced conductivity and charge mobility due to larger π-overlap, leading to greater π-orbitals from Se atoms and intermolecular Se-Se interactions. Furthermore, the larger size and lower electronegativity of Se compared to the chalcogenophene homolog of S result in selenophene-based polymers being more effective in broadening the absorption spectrum, particularly towards the infrared region. Based on the literature, it has been noted that the incorporation of selenophene units and benzothiophene acceptors can decrease the LUMO level while keeping the HOMO level constant. This modification has shown to significantly enhance the NLO properties of NF based compounds. Benzothiophene acceptors are valued in NLO applications for their extended conjugation aiding charge transfer, electron-accepting properties within D-π-A designs, structural impact on donor-acceptor separation, the potential for tailoring NLO properties, and their overall contribution to enhanced nonlinear optical responses in various applications.

In this study, we utilized **TATCN** [38] as a parent compound and modified it into a reference compound named as **DTPR**. In light of the prior research, we have designed a set of NF-based compounds labeled as **DTPD1-DTPD8**. These compounds were created by modifying **DTPR** through structural changes, involving altering the thiophene spacer group with selenophene and then the substitution of one donor (diphenylamine) with diverse strong electron-withdrawing acceptor moieties. The objective of our research is to establish a pronounced push-pull configuration [39,40]. Moreover, the DFT [41]-based NLO investigations of **DTPD1-DTPD8** have not been previously documented. To address this research gap, we utilized computational methods to scrutinize the NLO properties of these compounds. Our computational analyses encompassed parameters such as maximum absorbed wavelength (λ_{max}), NBO, FMO, GRP, β_{total} and γ_{total} for both the reference compound and its derivatives (**DTPD1-DTPD8**). It is our optimistic expectation that these designed compounds hold significant potential for enhancing NLO material performance.

2. Computational procedure

To analyze the key electronic structures, and NLO properties of fullerene free designed chromophores (**DTPD1–DTPD8),** the density functional theory (DFT [42]) and time-dependent DFT [43](TD-DFT) computations were applied. The optimization of molecular geometries in their ground state (S_0) was carried out without imposing symmetry restrictions. All computational calculations were executed using the Gaussian 09 program package [44] by utilizing the M06 functional [45] and 6-311G(d,p) basis set. The frontier molecular orbitals (FMOs) diagrams were generated with the assistance of Avogadro software [46]. This software facilitated the visualization of the highest occupied and lowest unoccupied molecular orbitals, as well as their corresponding energy levels. Additionally, global reactivity descriptors such as electronegativity (X), electron affinity (A), ionization potential (I), global electrophilicity index (ω), global softness (σ), chemical potential (μ) and global hardness (η) were calculated based on the energy gap between the HOMO and LUMO. An integral part of this scientific investigation involved the natural bond orbitals (NBOs) study, conducted using the NBO software package version 3.1 [47,48] in order to determine the stabilization patterns of the compounds under study. The density of states (DOS) analysis was conducted to assess the charge density of the designed compounds, employing the PyMOlyze 2.0 program [49]. The UV-Vis spectral analysis was accomplished using the TD-DFT method at the above mentioned level in dichloromethane, facilitated by the Origin [50] and Gauss Sum [49] software. Utilizing the previously stated functional, an assessment of the NLO properties for the specified chromophores was conducted. The determination of dipole moment (μ), average polarizability <α>, first hyperpolarizability (β_{total}), and second hyperpolarizability (γ_{total}) values involved the use of Equations 1-4 [51-54].

$$\langle \alpha \rangle = 1/3(\alpha_{xx} + \alpha_{yy} + \alpha_{zz}) \quad (1)$$

$$\beta_{total} = (\beta_x^2 + \beta_y^2 + \beta_z^2)^{1/2} \quad (2)$$

Where, $\beta_x = \beta_{xxx} + \beta_{xyy} + \beta_{xzz}$, $\beta_y = \beta_{yyy} + \beta_{xxy} + \beta_{yzz}$, $\beta_z = \beta_{zzz} + \beta_{xxz} + \beta_{yyz}$

$$\gamma_{total} = \sqrt{\gamma_x^2 + \gamma_y^2 + \gamma_z^2} \quad (3)$$

Where, $\gamma_i = \frac{1}{15}\sum_j (\gamma_{ijji} + \gamma_{ijij} + \gamma_{iijj}) \qquad i,j = \{x, y, z\}$

$$\mu = (\mu^2{}_x + \mu^2{}_y + \mu^2{}_z)^{1/2} \quad (4)$$

A comprehensive set of 10 hyperpolarizability tensors, including β_{xxx}, β_{xyy}, β_{xzz}, β_{yyy}, β_{xxy}, β_{yzz}, β_{zzz}, β_{xxz}, β_{yyz}, and β_{xyz}, were obtained as outputs from the Gaussian file, corresponding to the x, y and z directions.

3. Results and discussion

This study uses computational analysis to assess non-fullerene compounds for their suitability as efficient NLO materials. The compound (**TATCN**) [38], named as **DTPR** in this research, is taken as a reference compound with D-π-A-π-D configuration. In **DTPR**, thiophene [55] is replaced with the selenophene group (π-spacer) to produce **DTPD1** (first derivative) which also possess the same configuration as **DTPR.** As selenophene have higher polarizability, smaller energy band gaps and enhanced π electron conjugation making them more suitable for designing NLO materials with specific characteristics. The D-π-A_1-π-A_2 configuration is established in the second derivative (**DTPD2**) by replacing a terminal donor with conjugated acceptor in **DTPD1**. However, in case of **DTPD3-DTPD8**, acceptor 1, which initially contained a cyano group, was modified by removing the cyano group due to its tendency to trap charges. The remaining portion of acceptor 1 was then incorporated into the spacer. So, rest of the six derivatives (**DTPD3-DTPD8**) possess only one acceptor end *i.e.,* D-π-A framework. Within this scheme, the donor (diphenylamine) [56] and the π-spacer *i.e.,* 2,5-di (selenophen-2-yl) terephthalonitrile remain unchanged, while various derivatives are employed as the terminal acceptors. In this study, we analyze the HOMO and LUMO bandgap, $<a>$, β_{total} and γ_{total} of various acceptors. Fig. 1 provides an overview of the designed derivatives (**DTPD1-DTPD8**). Furthermore, Fig. 2 and S3 display the chemical structures and optimized configurations of the reference compound as well as the **DTPD1-DTPD8** derivatives. The comparative analysis between DFT and Experimental values of band length and bond angles was illustrated in Tables S44-S53. The cartesian coordinates of entitled chromophores were shown in Tables S1-S9.

3.1. Frontier molecular Orbitals

Frontier Molecular Orbitals (FMOs) play a pivotal role in the analysis of the intramolecular charge transfer (ICT) and optical properties of investigated organic molecules (**DTPR** and **DTPD1-DTPD8**) [57]. Quantum orbitals are referred to as the highest occupied molecular orbital (HOMOs) and the lowest unoccupied molecular orbital (LUMOs) reveal the efficiency of charge transfer within a molecule, typically from higher to lower energy levels [58]. HOMO functions as the electron source orbital, while LUMO, residing at a lower energy state, operates as the electron recipient molecular orbital [59]. The energy gap (E_{gap}) between these FMOs is a valuable indicator for assessing the chemical reactivity and dynamic stability of a material [60-62]. Molecules exhibiting a broader E_{gap} are generally regarded as more stable, less reactive and chemically hard nature. In contrast, molecules featuring a narrower E_{gap} are frequently viewed as less stable, highly reactive and soft in chemical nature, displaying increased polarizability and an exceptional NLO response [63,64].

In this study, we calculated the E_{gap} of the analyzed compounds using TD-DFT methodology with the help of M06/6-311G(d,p) level and the findings are detailed in the Table 1. Additionally, the energies differences of HOMO-1 and LUMO + 1 as well as HOMO -2 and LUMO +2 are provided in Table S10.

The HOMO/LUMO energy levels for **DTPR** are determined to be -5.588 and -2.468 *eV*, respectively, resulting in an E_{gap} value of 3.12 *eV*. In the case of **DTPD1-DTPD8**, the HOMO energy levels are found to be as -5.497, -5.748, -5.586, -5.590, -5.645, -5.701, -5621 and -5.646 *eV* respectively. Similarly, their associated LUMOs energy values are documented as follows: -2.440, -3.231, -3.182, -3.444, -3.430, -3.594, -3.248 and -3.399 *eV*, respectively. Furthermore, their corresponding E_{gap} values are 3.057, 2.517, 2.404, 2.146, 2.215, 2.107, 2.373 and 2.247 *eV*, respectively. In contrast to **DTPR**, all the other derivatives show a smaller E_{gap}, ranging from 2.107 to 3.057 *eV* which can be ascribed to the existence of strong electron-accepting substituents in their structure. Among all the chromophores, **DTPD6** showed the smallest E_{gap} (2.107 *eV*) due to the presence of sulphonic acid (-SO_3H) group which is highly electron-withdrawing in nature and can pull the electron density away from the surrounding atoms in a molecule. While, the widest band gap is shown by **DTPD1** (3.017 *eV*) as it not contains any electron accepting group in its structure. In remaining molecules, **DTPD2** possessed the reduced band gap than **DTPD1** (2.517<3.017 *eV*) due to the presence of floro (-F) group. Further, the band gap is reduced in case of **DTPD3** as compared to **DTPD1** due to removal of cyano group and replacement of floro group with chloro group in **DTP3** compound (2.404 *eV*). For **DTPD8**, which includes a cyano (-CN) group attached to the benzene ring and a malononitrile group on the thiophene ring, an increased band gap of 2.247 *eV* has been detected as compared to **DTPD5** which has nitro groups (-NO_2) on the terminal acceptor *i.e.,* 2.215 *eV*. **DPTD7** showed the reduced band gap than almost all derivatives except **DTPD6** due to the presence of acetate group in its structure which is more electronegative than carbon and exerts a strong electron-withdrawing effect on the benzene ring. In general, the energy gap trend is summarized as follows**: DTPD6 < DTPD4 < DTPD5 < DTPD8 < DTPD7 < DTPD3 < DTPD2 < DTPD1 < DTPR**.

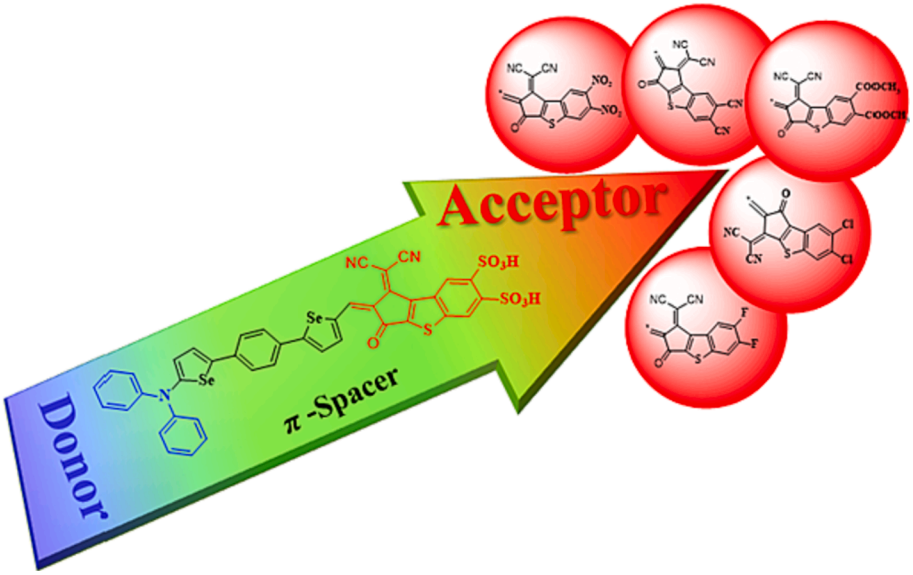

Fig. 1. Schematic representation of the investigated compounds.

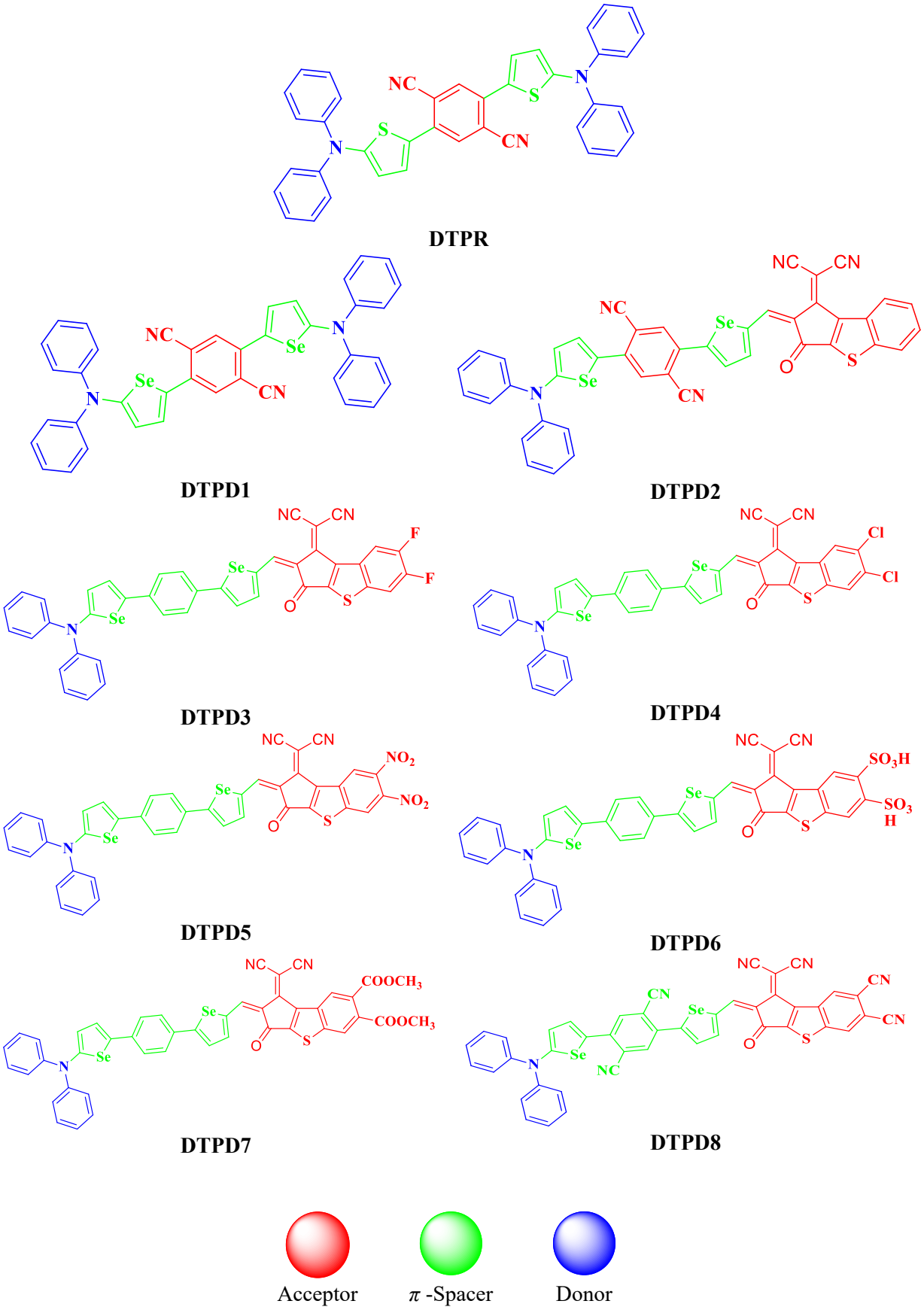

Fig. 2. The chemical structures of reference (**DTPR**) and designed compounds (**DTPD1-DTPD8**)

Table 1
The frontier molecular orbital energies of **DTPR** and **DTPD1-DTPD8**.

Compounds	E_{HOMO}	E_{LUMO}	Band Gap
DTPR	-5.588	-2.468	3.12
DTPD1	-5.497	-2.440	3.057
DTPD2	-5.748	-3.231	2.517
DTPD3	-5.586	-3.182	2.404
DTPD4	-5.590	-3.444	2.146
DTPD5	-5.645	-3.430	2.215
DTPD6	-5.701	-3.594	2.107
DTPD7	-5.621	-3.248	2.373
DTPD8	-5.646	-3.399	2.247

Band gap = $E_{LUMO}-E_{HOMO}$, units in *eV*.

The FMOs counter surface diagrams are illustrated in the Fig. 3 which clearly show the density of electrons in the form of clouds over different areas of the molecules. The reference compound (**DTPR**) shows different trend of electronic distribution due to its unique configuration and its HOMO is completely covered with electronic clouds. While, in case of its LUMO, the electronic clouds are majorly concentrated in the central region containing acceptor and spacers (see Fig. 3). Whereas, in derivatives (**DTPD2-DTPD8**), the HOMOs show electron density on their donor regions and partially over the π-spacer. In case of LUMOs, the acceptor part especially malonitrile over thiophene rings show prominent electronic clouds and also some of the charge is located on the spacer region.

The phenomena of charge transference can be depicted easily from

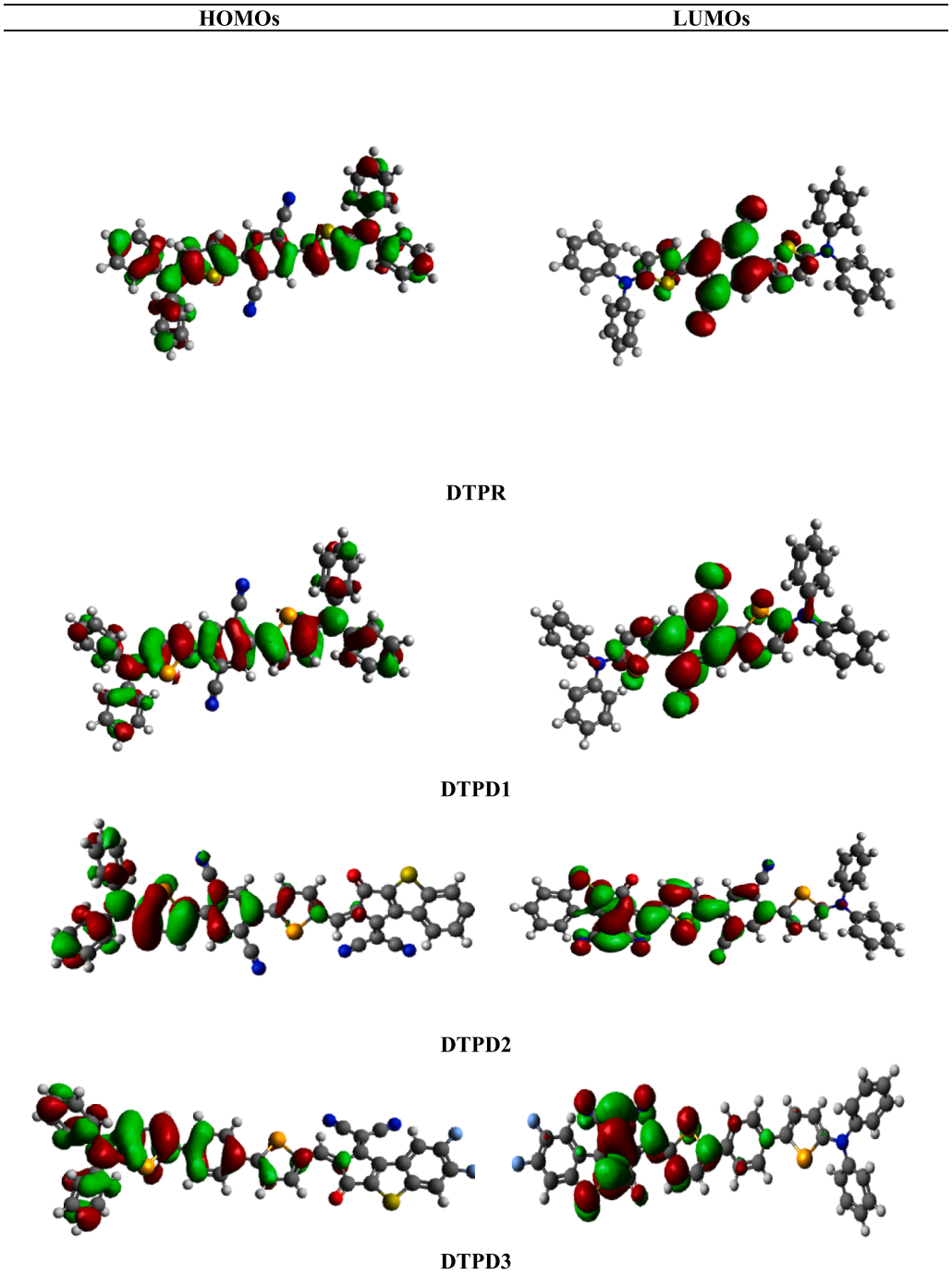

Fig. 3. HOMOs and LUMOs of the examined molecules (**DTPR** and **DTPD1-DTPD8**).

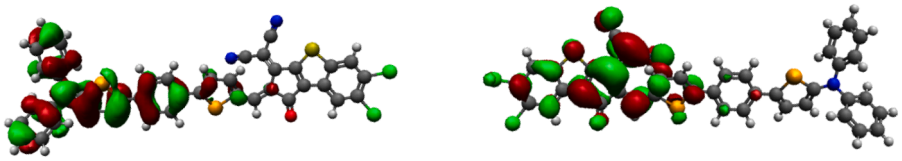

DTPD4

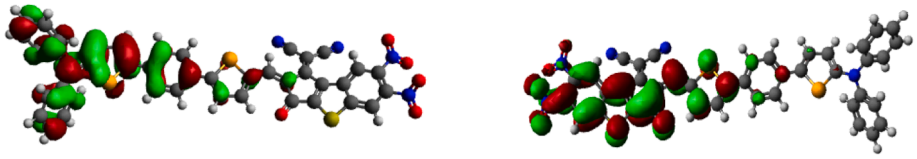

DTPD5

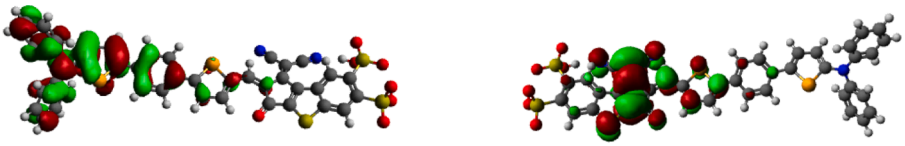

DTPD6

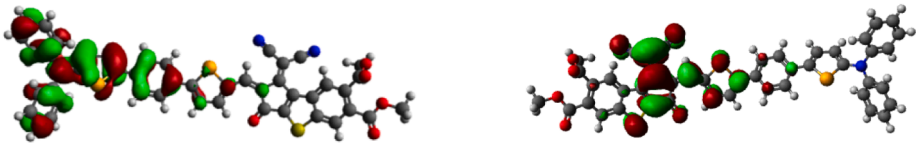

DTPD7

DTPD8

Fig. 3. (*continued*).

the energy values and FMOs diagram which help to predict the most suitable NLO design. The molecule (**DTPD4**) shows the lowest energy gap due to which it might be regarded as best NLO chromophore in the present computational simulation.

3.2. Global Reactivity Parameters

Utilizing the band gap alongside HOMO and LUMO energy levels allows us to assess reactivity and stability of entitled compounds, aiding in the prediction of their global reactivity parameters [32,65]. These include electronegativity (*X*) [66], ionization potential (*IP*) [67], global

softness (σ) [68], electron affnity (EA) [69], global hardness (η) [70], electrophilicity index (ω) [71] and chemical potential (μ) [72]. Koopman's theorem [73] was employed to establish these descriptors which are calculated according to the Equations 5-11.

$$IP = -E_{HOMO} \quad (5)$$

$$EA = -E_{LUMO} \quad (6)$$

$$X = \frac{[IP + EA]}{2} \quad (7)$$

$$\eta = IP - EA \quad (8)$$

$$\mu = \frac{E_{HOMO} + E_{LUMO}}{2} \quad (9)$$

$$\sigma = \frac{1}{\eta} \quad (10)$$

$$\omega = \frac{\mu^2}{2\eta} \quad (11)$$

The ability of a compound to absorb the more electrical charge from its environment is denoted by ΔN_{max} [74] and is calculated by the Equation 12.

$$\Delta N_{max} = -\mu/\eta \quad (12)$$

It has been observed that the compound's stability is directly affected by its hardness (η), whereas its reactivity is directly associated with its softness (σ). Compounds with high global hardness are stable and less reactive, while those with high global softness are more reactive and less stable. Table 2 illustrates that reference compound **(DTPR)** has the highest hardness value ($\eta = 1.56$ *eV*) as compared to its derivatives. Similarly, it possesses the lowest global softness value ($\sigma = 0.321$ *eV*), suggesting its higher stability and reduced reactivity. These characteristics resulted in a weaker NLO response for **DTPR**. Conversely, the designed compounds demonstrate lower hardness values (ranging from $\eta = 1.04$ to 1.53 *eV*) and global softness (ranging from ($\sigma = 0.327$ to 0.475 *eV*) in comparison to the **DTPR**. Among all the designed compounds, **DTPD6** is particularly notable for its smaller band gap of 2.107 *eV*, along with the highest softness value of 0.475 *eV* and the least hardness value of 1.04 *eV*, as specified in the Table 2. The softness values are arranged in decreasing order as follows: **DTPD6 > DTPD4 > DTPD5 > DTPD8 > DTPD7 > DTPD3 > DTPD2 > DTPD1 > DTPR**. The elevated softness values signify high reactivity and polarizability, which ultimately contribute to significant NLO behavior.

3.3. Natural Bond Orbital Analysis

To elucidate the nucleophilic and electrophilic hyper-conjugative interactions, along with other bonding interactions [75] and the electronic transition mechanisms, the NBO analysis stands out as the most precise and dependable technique [63]. It is a highly significant tool for analyzing charge transfer interactions between vacant and occupied molecular orbitals [49,76]. In D-π-A systems, it is frequently postulated that the electron-donating segment plays a primary role in charge transfer towards the electron-accepting segment. Thus, to elucidate the charge transfer phenomena within our designed compounds (**DTPD1-DTPD8**), we conducted NBO analysis on the optimized structures of **DTPD1-DTPD8** using the M06/6-311G(d,p) method. To assess reactions involving the delocalization, a second-order perturbation approach is utilized. Stabilization energy $E^{(2)}$ for each donor (i) to acceptor (j) transition, denoting the i → j delocalization, is calculated using the Equation (13).

$$E^{(2)} = q_i \frac{(F_{i,j})^2}{\varepsilon_j - \varepsilon_i} \quad (13)$$

In this Equation, the stabilization energy, denoted as $E^{(2)}$, relies on E_i and E_j, which are the diagonal elements of orbital energies. Additionally, q_i represents the occupancy of the donor orbital, while $F_{i,j}$ signifies the Fock matrix element between the natural bonding orbitals throughout the molecular structure [65]. The significant transitions involve: σ → σ*, π → π*, LP → σ* and LP → π*. In case of π-conjugated systems like our designed derivatives, the π → π* transitions are deemed the most pivotal for such organic NLO materials. Conversely, other types of allowed transitions, such as σ → σ*, are relatively weaker due to less pronounced interactions between the electron-rich donor and electron-deficient acceptor components. The primary values associated with these transitions are provided in the Table 3, while a more comprehensive analysis can be found in the supplementary information section (Tables S11–S19).

The highest π → π* transition in case of **DTPR** is 23.74 *kcal mol*$^{-1}$, which corresponds to π(C28-C30) → π*(C24-C26). Conversely, the π → π* transitions for the same compound are π(C45-C47) → π*(C11-C13) *i.e.,* 0.65 *kcal mol*$^{-1}$. In addition, the σ → σ* transition shows its maximum value with a stabilization energy of 8.54 *kcal mol*$^{-1}$ for σ(C5-C67) → σ*(C67-N68), while the minimum value for this transition occurs in σ(C9-C10) → σ*(C13-N21) *i.e.,* 0.61 *kcal mol*$^{-1}$. Furthermore, the LP2 → π* transition exhibits its highest energy of stabilization, reaching 25.87 *kcal mol*$^{-1}$, attributed to LP2(S71) → π*(C11-C13). Conversely, the highest value for LP1→ σ* transition is 12.45 *kcal mol*$^{-1}$, seen in LP1(N68) → σ*(C5–C67).

In molecules **DTPD1–DTPD8**, we observed favourable transitions with the highest stabilization energies. These transitions, namely π(C59-C63) → π*(C58-C61), π(C4-C5) → π*(C1-C6), π(C11-C13) → π*(C46-C48), π(C4-C5) → π*(C1-C6), π(C11–C13) → π*(C46-C48), π(C11-C13) → π*(C46-C48), π(C11-C13) → π*(C46-C48), and π(C11-C13) → π*(C46-C48) exhibit substantial values of 23.51, 24.46, 26.38, 25.42, 28.4, 29.1, 26.79, and 28.18 *kcal mol*$^{-1}$, respectively. These results strongly indicate the presence of conjugation in the tailored compounds.

Conversely, the transitions involving π(C45-C47) → π*(C11-C13), π(C45-C47) → π*(C11-C13), π(C58-C60) → π*(C58-C60), π(C9-C10) → π*(C9-C10), π(C49-C64) → π*(C65-N66), π(C22-C24) → π*(C17-C19), π(C33-C34) → π*(C22-C24), π(C52-C53) → π*(C56-N57), and π(C9-C10) → π*(C46–C48) are characterized by the lowest stabilization energies, measuring 0.65, 0.5, 0.56, 0.5, 0.67, 0.51, 0.52, and 0.67 *kcal mol*$^{-1}$, respectively.

Table 2
Global reactivity parameters for the investigated compounds (**DTPR** and **DTPD1-DTPD8**).

Compound	*X*	*μ*	*η*	*σ*	*ω*	*I.P*	*E.A*	ΔN_{max}
DTPR	4.028	-4.028	1.56	0.321	5.200	5.588	2.468	-2.582
DTPD1	3.969	-3.969	1.53	0.327	5.152	5.497	2.44	-2.596
DTPD2	4.490	-4.490	1.26	0.397	8.008	5.748	3.231	-3.563
DTPD3	4.384	-4.384	1.20	0.416	7.995	5.586	3.182	-3.653
DTPD4	4.517	-4.517	1.07	0.466	9.507	5.59	3.444	-4.210
DTPD5	4.538	-4.538	1.11	0.451	9.295	5.645	3.43	-4.088
DTPD6	4.647	-4.647	1.04	0.475	10.25	5.701	3.594	-4.468
DTPD7	4.435	-4.435	1.18	0.421	8.287	5.621	3.248	-3.758
DTPD9	4.522	-4.522	1.12	0.445	9.102	5.646	3.399	-4.038

Units are in *eV*.

Table 3
Natural bond orbital (NBOs) analysis of **DTPR** and **DTPD1-DTPD8** compounds.

Compound	Donor(*i*)	Type	Acceptor(*j*)	Type	$E^{(2)}$ [*kcal/mol*]	$E_{(j)}$-$E_{(i)}$ [*a.u*]	$F_{(i,j)}$ [*a.u*]
DTPR	C28-C30	π	C24-C26	π*	23.74	0.3	0.075
	C45-C47	π	C11-C13	π*	0.65	0.28	0.012
	C5-C67	σ	C67-N68	σ*	8.54	1.61	0.105
	C9-C10	σ	C13-N21	σ*	0.61	1.18	0.024
	S71	LP(2)	C11-C13	π*	25.87	0.27	0.075
	N68	LP(1)	C5-C67	σ*	12.45	1.04	0.102
	C59-C63	π	C58-C61	π*	23.51	0.3	0.075
	C45-C47	π	C11-C13	π*	0.65	0.28	0.012
DTPD1	C5-C67	σ	C67-N68	σ*	8.54	1.61	0.105
	C15-Se72	σ	C16-C17	σ*	0.54	1.17	0.023
	N21	LP(1)	C11-C13	π*	28.35	0.29	0.083
	N70	LP(1)	C2-C69	σ*	12.46	1.05	0.102
	C4-C5	π	C1-C6	π*	24.46	0.3	0.077
	C58-C60	π	C58-C60	π*	0.5	0.28	0.011
DTPD2	C5-C70	σ	C70-N71	σ*	8.57	1.61	0.105
	C56-N57	σ	C50-C51	σ*	0.5	1.64	0.026
	N19	LP(1)	C15-C17	π*	38.52	0.29	0.097
	O52	LP(2)	C47-C48	σ*	21.36	0.75	0.114
	C11-C13	π	C46-C48	π*	26.38	0.31	0.081
	C9-C10	π	C9-C10	π*	0.56	0.3	0.012
DTPD3	C53-C56	σ	C56-N57	σ*	8.42	1.61	0.105
	S55-C62	σ	C65-H67	σ*	0.5	1.07	0.021
	S55	LP(2)	C50-C51	π*	29.48	0.27	0.081
	O54	LP(2)	C49-C50	σ*	21.52	0.74	0.114
	C4-C5	π	C1-C6	π*	25.42	0.29	0.077
	C49-C64	π	C65-N66	π*	0.5	0.42	0.014
DTPD4	C46-H47	σ	C48-C49	σ*	9.41	1.01	0.087
	C9-Se44	σ	C10-C11	σ*	0.51	1.2	0.022
	S53	LP(2)	C50-C51	π*	27.1	0.28	0.078
	O69	LP(2)	C48-C52	σ*	22.24	0.71	0.114
	C11-C13	π	C46-C48	π*	28.4	0.31	0.084
	C22-C24	π	C17-C19	π*	0.67	0.29	0.012
DTPD5	C53-C56	σ	C56-N57	σ*	8.45	1.61	0.105
	C46-C48	σ	C11-C13	σ*	0.5	1.33	0.023
	O71	LP(3)	O70-N74	π*	161.42	0.18	0.154
	N21	LP(1)	C17-C19	σ*	22.27	0.87	0.043
	C11-C13	π	C46-C48	π*	29.1	0.3	0.084
	C33-C34	π	C22-C24	π*	0.51	0.3	0.011
DTPD6	C53-C56	σ	C56-N57	σ*	8.98	1.63	0.109
	C46-C48	σ	C63-S70	σ*	0.5	1.18	0.023
	S55	LP(2)	C50-C51	π*	29.28	0.27	0.081
	O54	LP(2)	C49-C50	σ*	22.52	0.73	0.116
	C11-C13	π	C46-C48	π*	26.79	0.31	0.082
	C52-C53	π	C56-N57	π*	0.52	0.41	0.014
DTPD7	C53-C56	σ	C56-N57	σ*	8.54	1.62	0.105
	S55-C62	σ	C62-C65	σ*	0.5	1.26	0.023
	O74	LP(2)	C71-O73	π*	49.43	0.37	0.122
	O73	LP(2)	C71-O74	σ*	34.16	0.67	0.137
	C11-C13	π	C46-C48	π*	28.18	0.31	0.083
	C9-C10	π	C9-C10	π*	0.67	0.3	0.013
DTPD8	C66-C72	σ	C72-N73	σ*	8.97	1.62	0.108
	C46-C48	σ	C11-C13	σ*	0.51	1.33	0.023
	S55	LP(2)	C50-C51	π*	29.27	0.27	0.081
	O54	LP(2)	C49-C50	σ*	22.08	0.73	0.115

In the case of σ → σ* transitions, such as σ(C5-C67) → σ*(C67-N68), σ(C5-C70) → σ*(C70-N71), σ(C53-C56) → σ*(C56-N57), σ(C46-H47) → σ*(C48-C49), σ(C53-C56) → σ*(C56-N57), σ(C53–C56) → σ*(C56-N57), σ(C53-C56) → σ*(C56-N57), and σ(C66-C72) → σ*(C72-N73), we observe higher stabilization energies, with values of 8.54, 8.57, 8.42, 9.41, 8.45, 8.98, 8.54, and 8.97 *kcal mol*$^{-1}$ for **DTPD1–DTPD8**, respectively. Conversely, the transitions associated with the lowest energy values in σ → σ* transitions are as follows: σ(C15-Se72) → σ*(C16-C17) at 0.54 *kcal mol*$^{-1}$, σ(C56-N57) → σ*(C50-C51) at 0.5 *kcal mol*$^{-1}$, σ(S55–C62) → σ*(C65–H67) at 0.5 *kcal mol*$^{-1}$, σ(C9-Se44) → σ*(C10-C11) at 0.51 *kcal mol*$^{-1}$, σ(C46-C48) → σ*(C11-C13) at 0.5 *kcal mol*$^{-1}$, σ(C46-C48) → σ*(C63-S70) at 0.5 *kcal mol*$^{-1}$, σ(S55-C62) → σ*(C62-C65) at 0.5 *kcal mol*$^{-1}$, and σ(C46-C48) → σ*(C11-C13) at 0.51 *kcal mol*$^{-1}$, all for **DTPD1–DTPD8**, respectively.

Furthermore, in the context of resonance, we observe transitions like LP1(N21) → π*(C11-C13), LP1(N19) → π*(C15-C17), LP2(S55) → π*(C50-C51), LP2(S53) → π*(C50-C51), LP3(O71) → π*(O70-N74), LP2(S55) → π*(C50-C51), LP2(O74) → π*(C71-O73), and LP2(S55) → π*(C50-C51). These transitions are characterized by stabilization energies of 28.35, 38.52, 29.48, 27.1, 161.42, 29.28, 49.43, and 29.27 *kcal mol*$^{-1}$in **DTPD1–DTPD8**, respectively. We also observe additional lone pair transitions, including LP1(N70) → σ*(C2-C69), LP2(O52) → σ*(C47-C48), LP2(O54) → σ*(C49-C50), LP2(O69) → σ*(C48-C52), LP1(N21) → σ*(C17-C19), LP2(O54) → σ*(C49-C50), LP2(O73) → σ*(C71-O74), and LP2(O54) → σ*(C49-C50). These transitions exhibit major stabilization energies of 12.46, 21.36, 21.52, 22.24, 22.27, 22.52, 34.16, and 22.08 *kcal mol*$^{-1}$, respectively.

Additionally, the findings highlight the substantial contribution of delocalized π-electrons within the C-C bonding [77] orbitals to both the stabilization and overall structural configuration of the compounds. Consequently, the extended hyperconjugation observed in these chromophores plays a pivotal role in the stabilization of these compounds,

significantly amplifying their NLO response.

3.4. Density of states

Density of states plots are employed to elucidate the findings derived from FMO analysis when exploring impact of acceptor groups in the

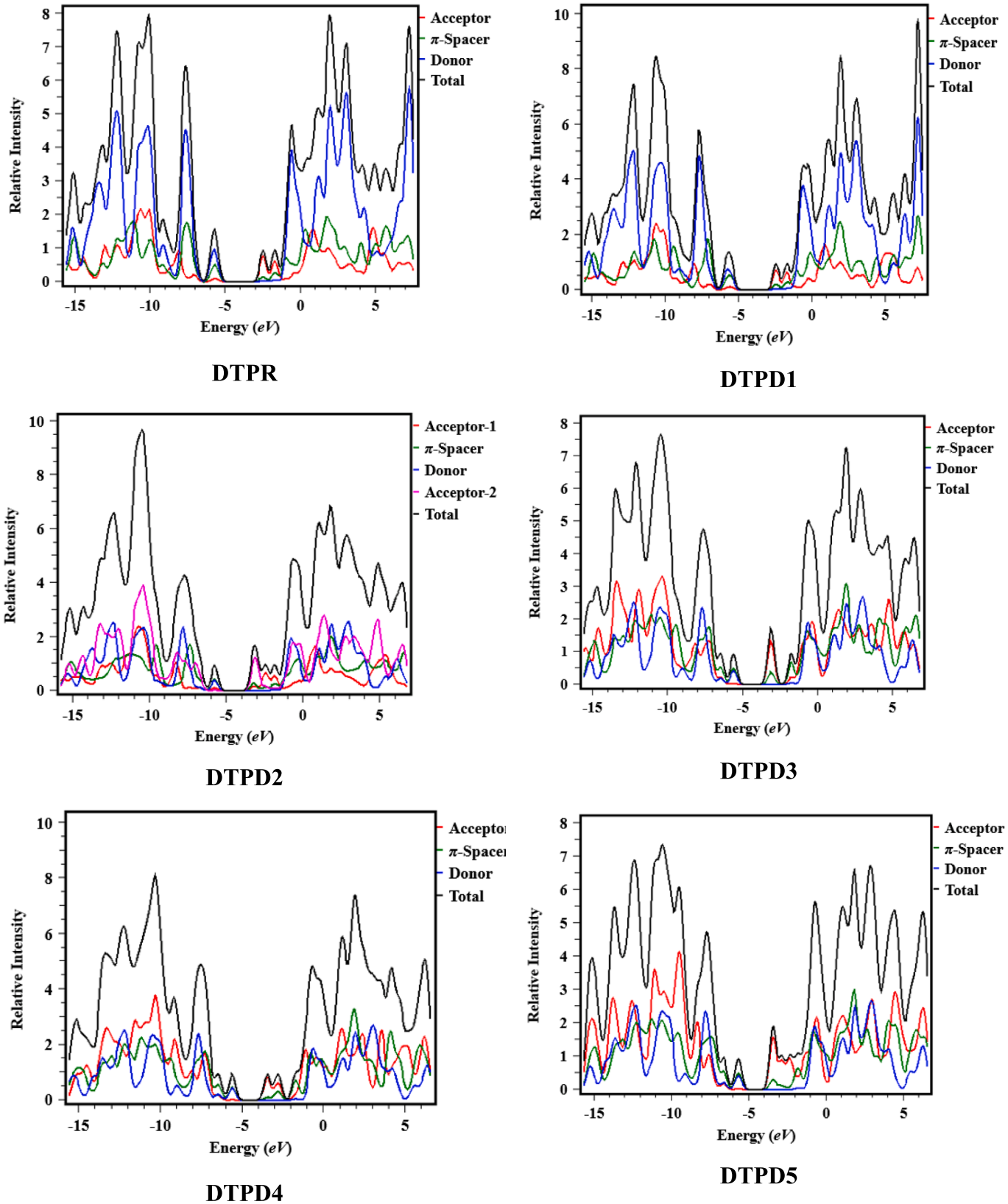

Fig. 4. DOS plots for **DTPR** and **DTPD1 to DTPD8**.

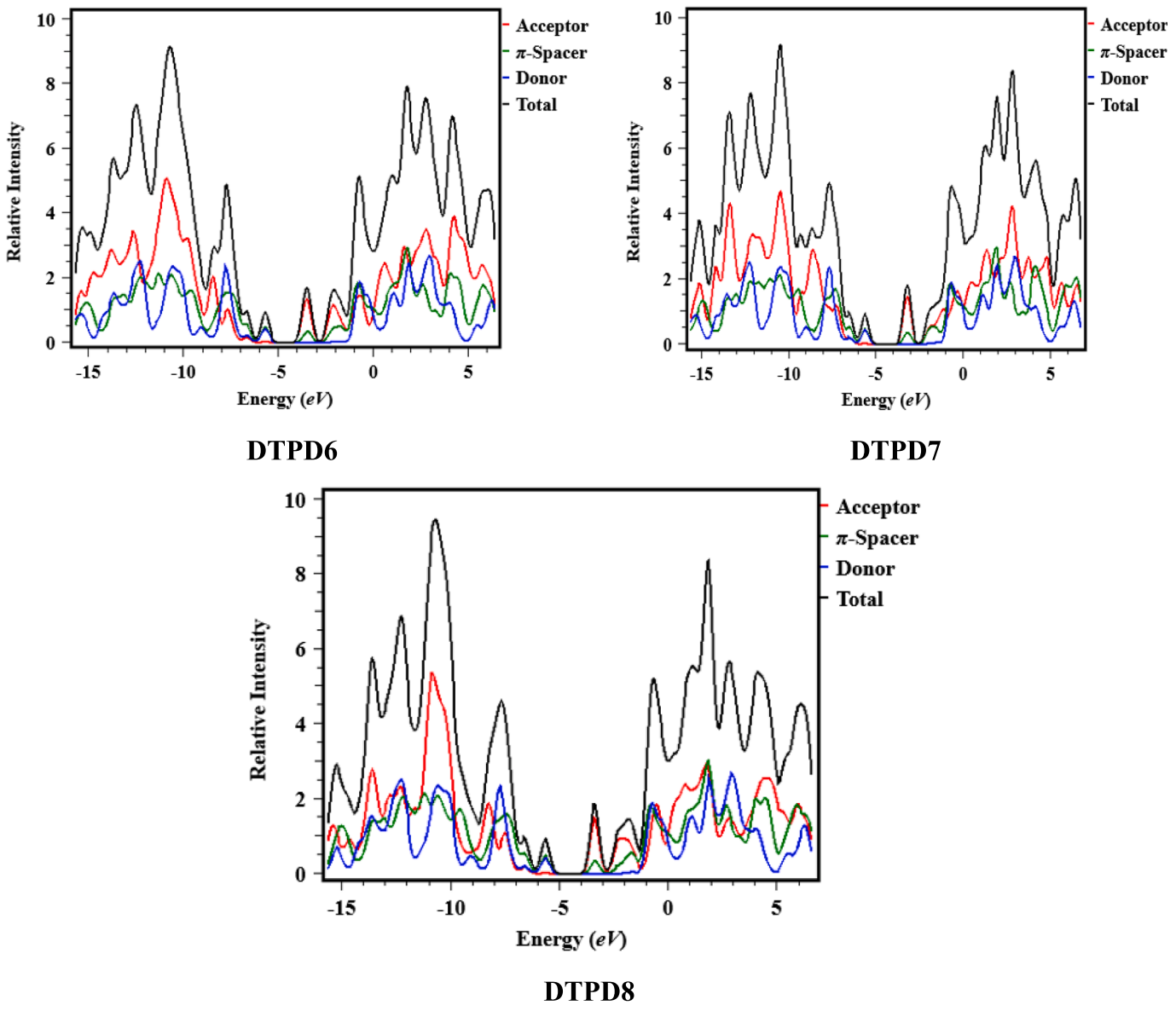

Fig. 4. (*continued*).

designed molecules [78] (**DTPR** and **DTPD1-DTPD8**). The analysis of DOS can unveil the electron density distribution from the HOMOs, known for their strong electron-donating characteristics, to the LUMOs, which are recognized for their pronounced electron-accepting attributes [79]. The graph depicted in the Fig. 4 illustrates that on the x-axis, negative values correspond to the valence band (HOMO), whereas positive values represent the conduction band (LUMO). The energy gap is the measure of the separation distance between the HOMO and LUMO. In the context of DOS analysis, we divided our compound (**DTPD1**) into three segments namely donor, spacer, acceptor. While, **DTPD2** is fragmented into four regions as donor, spacer, acceptor 1 and acceptor 2 and other derivatives (**DTPD3-DTPD8**) into three distinct segments, namely acceptor, spacer and donor. The electronic distribution pattern exhibited by the donor, spacer and acceptor in **DTPD1** 46.6, 43.4, 10.0% to HOMO and 3.6, 21.4, 75.0% to LUMO. In **DTPD2**, the electronic dispersion pattern contributes 40.4, 45.4, 12.0, 2.2% towards HOMO and 0.8, 25.7, 14.2, 59.4% towards LUMO by donor, spacer, acceptor 1 and acceptor 2 respectively.

The acceptors exhibited a distribution pattern of electronic charge for **DTPD3-DTPD8** as follows: 44.6, 47.0, 44.5, 46.0, 46.9 and 44.9 % of the charge was directed towards the HOMOs, while 0.3, 0.1, 0.3, 0.2, 0.2 and 0.1 % was assigned to the LUMOs, respectively. The π-linker donates 52.5, 50.6, 52.6, 51.1, 50.6 and 52.3 % to HOMOs and 19.7, 11.6, 19.1, 12.9, 15.6 and 10.2 % to LUMOs and acceptor accounts 2.9, 2.4, 2.9, 2.8, 2.5 and 2.8 % for HOMOs and 80.1, 88.3, 80.6, 86.9, 84.2 and 89.6% for LUMOs in **DTPD3-DTPD8** respectively. Additionally, the FMOs analysis of the examined compounds demonstrated that, for all of them, the HOMO exhibited substantial electron density localized on the spacer and donor. When examining the LUMO, it's notable that the electron density primarily resides on the acceptor 2 in the case of **DTPD2**, as it contains two acceptors. For all the remaining compounds, the electron density is predominantly concentrated on the acceptor 9 Fig. 4). The DOS analysis of **DTPR** and its derivatives (**DTPD1-DTPD8**) indicates efficient electron transfer from donor groups to acceptors through the π-bridge, enhancing the push-and-pull mechanism.

3.5. Transition density matrix (TDM) and binding energy (E_b) analysis

TDM analysis plays a crucial role in investigating how charge is transferred and the mode of interaction among acceptor, donor and π-spacer fragments in all the investigated compounds [80]**.** Moreover, it is a useful method for quantifying changes in charge distribution upon

excitation, characterizing the degree of electron-hole pair confinement or dispersal and unraveling the interplay between entities which accept electrons and those which donate electrons in an excited state [81,82]. This analysis visually illustrates the interactions [83] between the donor and acceptor using three-dimensional plots which incorporate a wide range of colors for clear representation [84]. In this study, the influence

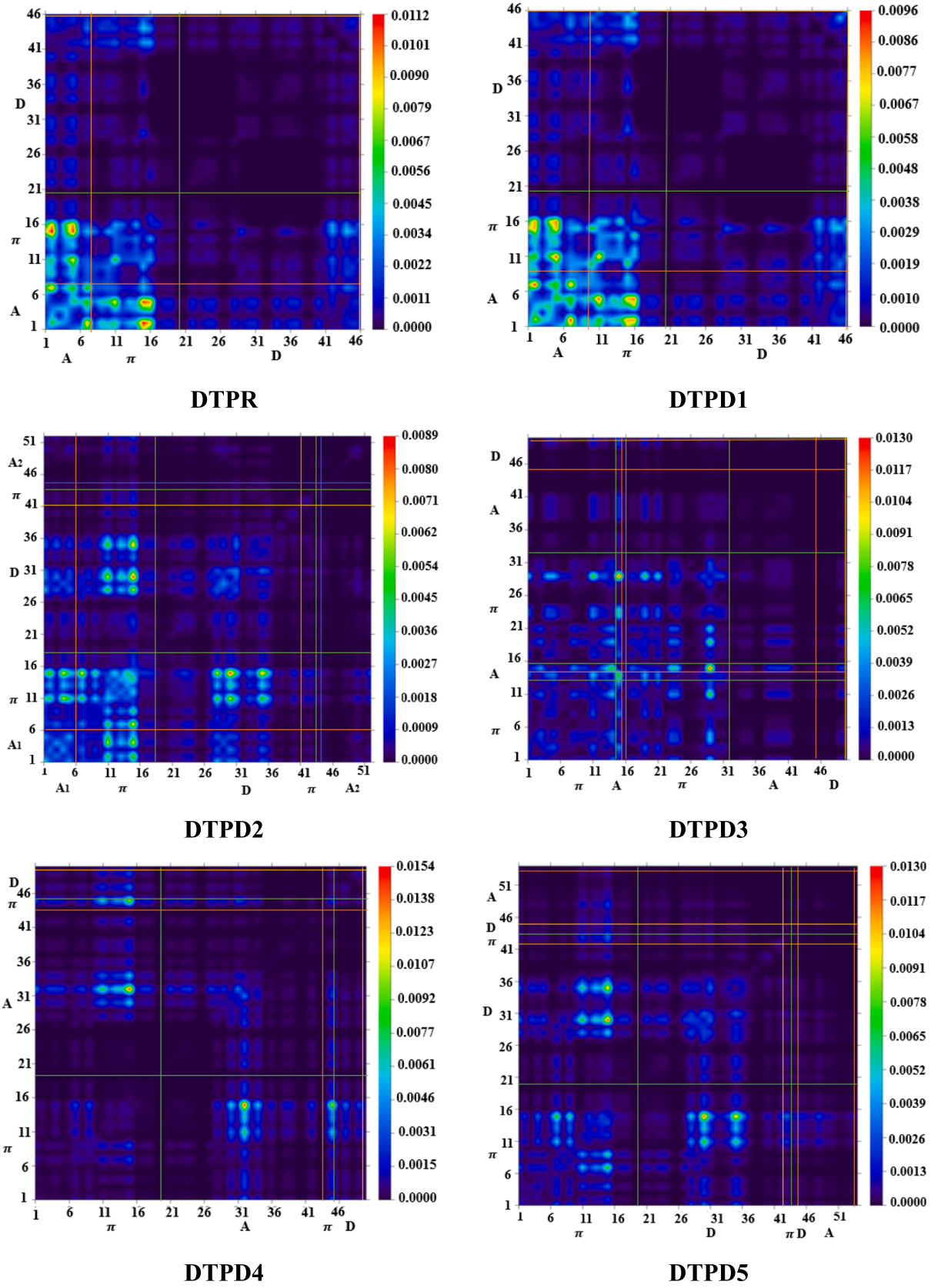

Fig. 5. TDM plots illustration for **DTPR** and **DTPD1-DTPD8**.

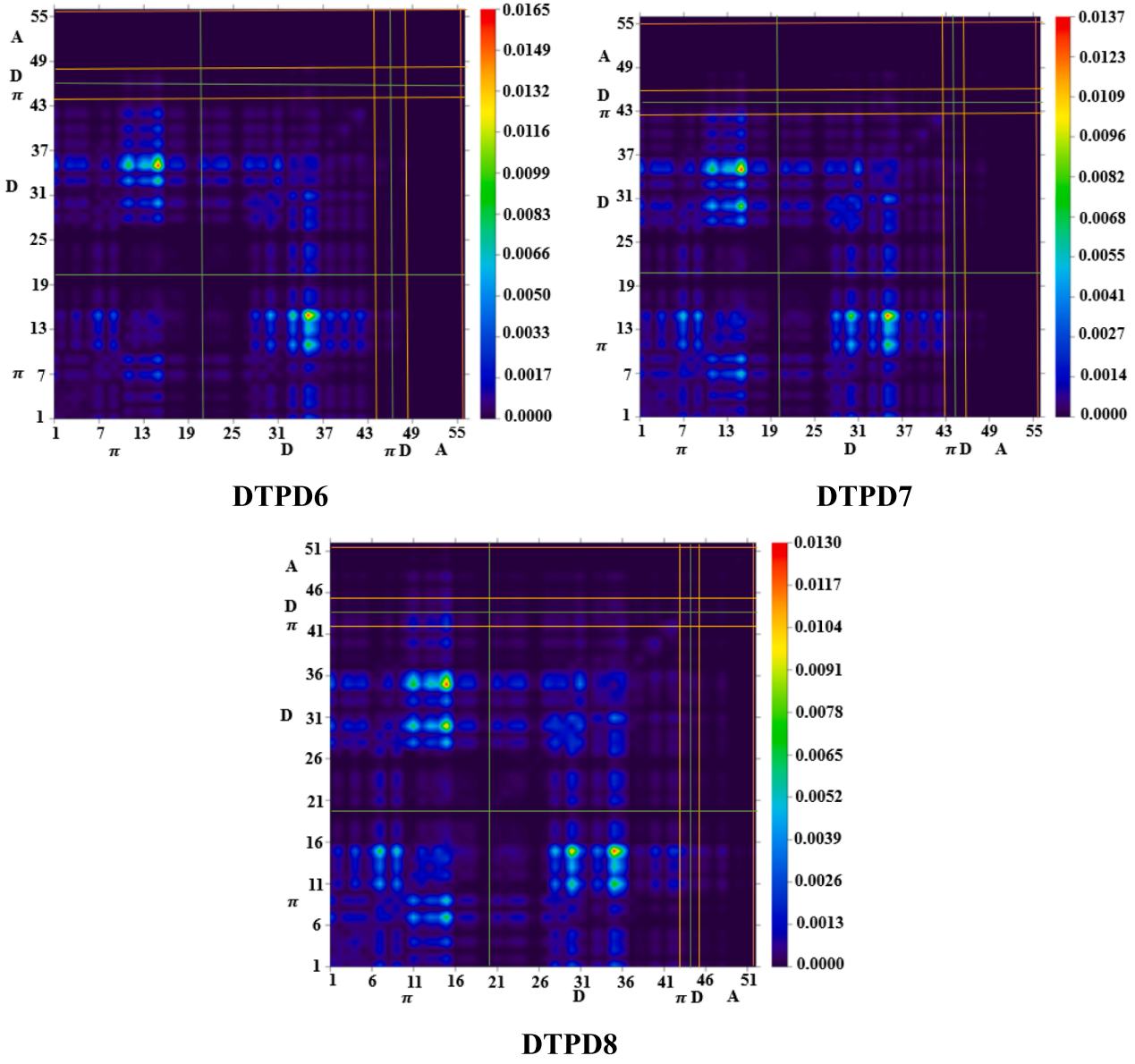

Fig. 5. (*continued*).

of hydrogen (H) atom is disregarded because of its minimal contribution to the transitions. Figure 5 showcases the TDM results for both the reference compounds and their derivatives analyzed in this study.

Taking into account the electronic charge transfer, we divided the compounds we examined in three segments: donor, π-spacer and acceptor. In Figure 5, it is observed that molecules with distinct fragments are positioned along the bottom and left sides, while electron density is indicated on the right y-axis. TDM images, validate that electrons undergo efficient transfer from the π-spacer to the acceptor, thereby enabling unrestricted electron flow throughout the molecule. The findings from the TDM heat maps indicate a distinct spatial segregation in the excited transition state, which holds significant importance for development of nonlinear optical materials.

The difference between electrical and optical band gap energies is known as binding energy (E_b), a key factor in evaluating the NLO features of designed compounds. The Equation (14) is utilized to calculate the E_b of both the reference and engineered chromophores.

$$E_b = E_{L-H} - E_{opt} \tag{14}$$

Here, the E_b represents the binding energy, E_{L-H} refers to the band gap between HOMO and LUMO and E_{opt} represents the first excitation energy [85]. The computed binding energy results are presented in the Table 4.

Table 4 demonstrates that entitled compounds have binding energies ranging from 1.142 to 2.295 *eV*, all of which are less than **DTPR** (2.389 *eV*). The observed values could be a result of the configuration changes

Table 4
Computed excitation binding energy (E_b) of the entitled chromophores (**DTPR** and **DTPD1-DTPD8**).

Compounds	E_{H-L}	E_{opt}	E_b
DTPR	3.12	0.731	2.389
DTPD1	3.057	0.762	2.295
DTPD2	2.517	1.170	1.347
DTPD3	2.404	0.845	1.559
DTPD4	2.146	0.916	1.230
DTPD5	2.215	1.073	1.142
DTPD6	2.107	0.585	1.522
DTPD7	2.373	0.949	1.424
DTPD8	2.247	0.983	1.264

Units are in *eV*.

that create a robust push-pull orientation. **DTPD1** exhibits the highest binding energy (E_b) value at 2.295 *eV*, which is very close to that of the reference molecule. This similarity is noteworthy because **DTPD1** lacks any acceptor or electron-withdrawing groups in its structure. The reduced binding energy, coupled with smaller first excitation energy and energy gap values, promotes more efficient exciton dissociation and notably higher charge mobility, resulting in enhanced optoelectronic [86,87] properties. The general decreasing order of binding energies for both the reference and investigated compounds is as follows: **DTPR > DTPD1 > DTPD3 > DTPD6 > DTPD7 > DTPD2 > DTPD8 > DTPD4 > DTPD5**. Binding energy is associated with polarizability and materials characterized by lower binding energy are often deemed as excellent photonic compounds due to their remarkable NLO properties [20]. Notably, the lowest binding energy (1.142 *eV*) observed in **DTPD5**, due to its high conduction rate and ease of segregating into individual charges, designates it as an outstanding material for NLO applications.

3.6. Nonlinear optical analysis

Enhanced NLO properties in various materials hold significant promise for advancing applications in emerging areas like harmonic generation, electro-optic modulation, frequency mixing and communication technologies [82,88,89]. Therefore, a comprehensive understanding of NLO properties is essential for the development of such materials. To generate inherent nonlinear optical properties, a push-pull type structure is essential. This structure can be created by strategically incorporating suitable donor and acceptor units at specific locations, and its effectiveness can be enhanced by extending conjugation through the inclusion of π-spacers [90]. The magnitude of the optical response is dictated by the electronic characteristics of the material, which are influenced by factors such as $\langle\alpha\rangle$, β_{tot} and γ_{tot} and μ_{tot}.

The dipole moment is particularly affected by the electronegativity of molecules. Stronger electronegativity in a system is reflected by higher dipole moment values. Polarity and dipole moment are crucial for enhancing a molecule's NLO potential [91]. The computed dipole moment (μ_{tot}) along with the tensors (μ_x, μ_y and μ_z) data for the studied compounds (**DTPR** and **DTPD1–DTPD8**) are recorded in the Table S20. It is clearly seen that the dipole moment tensor along the x-axis (μ_x) predominantly contributes to the μ_{tot} values, whereas the values along the z and y-axes (μ_y and μ_z) show relatively lesser contribution. The dipole moment values for our series of compounds are ranked as follows: **DTPD6** (20.135 *D*) > **DTPD5** (17.694 *D*) > **DTPD7**= **DTPD8** (14.678 *D*) > **DTPD3** (10.128 *D*) > **DTPD2** (8.578 *D*) > **DTPD4** (6.661 *D*) > **DTPD1** (0.593 *D*). Notably, the derivative **DTPD6** possesses the highest value (20.135 *D*), signifying it as the most polarized molecule. A review of the literature highlights the use of the para-nitroaniline (p-NA) molecule as a reference for comparative NLO studies [92]. Notably, the dipole moments of all these molecules exceed that of para-nitroaniline (p-NA), which has a value of 4.962 *D*, except **DTPD1**, as it lacks any accepting group or electronegative atom in its structure.

Similarly, the linear polarizability $\langle\alpha\rangle$ serves as an effective descriptor of the electronic properties and polarity of compounds. The $\langle\alpha\rangle$ values, along with their primary contributing tensors (α_{xx}, α_{yy} and α_{zz}) are listed in the Table S21, while the key values are presented in the Table 5 of the manuscript, with all parameters measured in *esu* units. The dominant values within the average polarizability tensor are found along the x-axis (α_{xx}), indicating that the overall polarizability $<\alpha>$ is aligned in this direction. The literature indicates that a molecule's polarizability is greatly affected by the energy gap between its HOMO and LUMO. Molecules with smaller energy gap values typically display higher linear polarizability and vice versa. In the series of designed chromophores, **DTPD1** demonstrates the least $\langle\alpha\rangle$ value (1.079×10^{-22} *esu*), whereas, **DTPD6** stands out as the most polarizable derivative, showcasing a significant linear polarizability value of 1.561×10^{-22} *esu*. Interestingly, all of these compounds possess considerably higher linear polarizability values than both the reference molecule **DTPR** and the standard *p*-NA molecule ($\langle\alpha\rangle = 1.173\times10^{-24}$ *esu*), demonstrating their exceptional NLO response.

Table 5
Computed dipole moment (μ_{tot}), average linear polarizability $\langle\alpha\rangle$, first (β_{tot}) and second hyper-polarizability $\langle\gamma\rangle$ of **DTPR** and **DTPD1-DTPD8**.

Compounds	μ_{tot}	$\langle\alpha\rangle\times10^{-22}$	$\beta_{tot}\times10^{-27}$	$\gamma_{tot}\times10^{-32}$
DTPR	0.319	1.009	0.006	0.153
DTPD1	0.593	1.079	0.016	0.198
DTPD2	8.578	1.410	1.003	0.899
DTPD3	10.128	1.360	1.186	1.077
DTPD4	6.661	1.388	1.081	1.204
DTPD5	17.694	1.502	2.038	1.961
DTPD6	20.135	1.561	2.111	1.952
DTPD7	14.678	1.479	1.314	1.225
DTPD8	14.678	1.504	1.893	1.775

Dipole moment (μ_{tot}) in Debye (D) while, $\langle\alpha\rangle$, first hyper-polarizability(β_{tot}) and second hyper-polarizability $\langle\gamma\rangle$ in *esu* units.

The first-hyper-polarizability (β_{tot}) plays a vital role in assessing the non-linear optical properties of a chromophore. The β_{tot} can be determined through the utilization of nine contributing tensors (β_{xxx}, β_{xxy}, β_{xyy}, β_{yyy}, β_{xxz}, β_{yyz}, β_{xzz}, β_{yzz} and β_{zzz}). The β_{tot} values and their tensors are calculated for the designed compounds *i.e.,* **DTPD1-DTPD8**, and the comprehensive results are presented in the Table S22. While, the representative β_{tot} values are also tabulated in the manuscript (see Table 5) yielding the following results: 0.016, 1.003, 1.186, 1.081, 2.038, 2.111, 1.314 and 1.893×10^{-27} *esu*, respectively. Compound (**DTPD6**) shows the highest value as 2.111×10^{-27} *esu* among all compounds under study. The enhanced β_{tot} can be attributed to the robust push-pull configuration and the incorporation of electron-withdrawing groups in the customized chromophore, resulting in a higher value. Significantly, the tailored chromophores containing additional electron-withdrawing groups, such as -SO_3H, -NO_2 and -CN in **DTPD6**, **DTPD5** and **DTPD8** respectively, exhibit elevated first-hyper-polarizability values.

The Table S23 displays the calculated second hyperpolarizability γ_{tot} values for designed derivatives, which was obtained using the M06 method with a 6-311G (d,p) basis set. Based on the acquired data, it's evident that the primary contribution to the $\langle\gamma\rangle$ values originate from the second hyperpolarizability tensor along the x-axis (γ_x) in all considered chromophores. Similarly, when comparing the second hyper-polarizability values of all the specified chromophores to p-NA, it was observed that all the examined chromophores exhibited greater efficiency than the standard *p*-NA (with a value of 2.75×10^{-36} *esu*). Based on the preliminary data, the ultimate findings for the third-order NLO parameter reveal that **DTPD5**, **DTPD6**, and **DTPD6** exhibit the highest γ_{tot} values, measuring at 1.979×10^{-32}, 1.971×10^{-32} and 1.790×10^{-32} *esu*, respectively. **DTPD6** and **DTPD5** emerged as the top performers among all the candidates in terms of their favorable $\langle\alpha\rangle$, β_{tot} and γ_{tot} values.

3.7. UV-Vis investigations

Utilizing UV-Vis spectroscopy [93,94], we employed TD-DFT computations with the M06/6-311G(d,p) combination to elucidate the absorption spectra pertaining to the excited states in **DTPR** and **DTPD1-DTPD8.** This analysis enabled us to detect details about the probability of charge transfer, the configurations that drive these transitions [95], and the inherent nature of the electronic transitions in these systems [96-98]. Tables 6 and 7 present the calculations for the maximum absorption wavelength (λ_{max}), excitation energies (*E*), oscillation strengths (f_{os}), and contributions from molecular orbitals for the studied compounds. Figure 6 and Tables S24-43 illustrates the absorption spectra of the designed compounds, revealing absorbance within the visible spectrum.

In a dichloromethane solvent, the **DTPD6** compound demonstrates

Table 6
Transition energy (*E*), λ_{max}, f_{os} and MO participation of entitled molecules **DTPR** and **DTPD1- DTPD8** in Dichloromethane.

Medium	System	λ_{max} (*nm*)	E (*eV*)	f_{os}	MO contributions
Dichloromethane	**DTPR**	395.560	3.134	0.731	H→L+1 (94%), H-1→L+2 (3%)
	DTPD1	527.032	2.353	0.762	H→L (97%)
	DTPD2	605.806	2.047	1.170	H→L (89%), H→L+1 (5%)
	DTPD3	622.661	1.991	0.845	H→L (88%), H→L+1 (6%)
	DTPD4	527.660	2.350	0.916	H→L+1 (60%), H-1→L (28%)
	DTPD5	678.139	1.828	1.073	H→L (49%), H→L+1 (46%)
	DTPD6	712.307	1.741	0.585	H→L (92%), H→L+1 (4%)
	DTPD7	452.530	2.740	0.949	H-1→L+1 (80%), H-1→L (8%)
	DTPD8	667.946	1.856	0.983	H→L (59%), H→L+1 (37%)

fos= oscillator strength, H=HOMO, L=LUMO, MO=molecular orbital.

Table 7
Transition energy (*E*), λ_{max}, f_{os} and MO participation of entitled molecules **DTPR** and **DTPD1- DTPD8** in Gaseous phase.

Medium	System	λ_{max} (*nm*)	*E* (*eV*)	f_{os}	MO contributions
Gaseous	**DTPD1**	507.3	2.444	0.665	H→L (97%)
	DTPD2	578.4	2.144	1.01	H→L (93%), H→L+1 (2%)
	DTPD3	430.8	2.878	0.909	H-1→L+1 (71%), H-1→L (17%)
	DTPD4	514.4	2.41	0.544	H-1→L (73%), H→L+1 (16%)
	DTPD5	654.4	1.895	0.838	H→L+1 (84%), H→L (14%)
	DTPD6	457.3	2.711	1.045	H-1→L+1 (80%), H-1→L (7%)
	DTPD7	440.8	2.812	1.122	H-1→L+1 (69%), H-1→L (19%)
	DTPD8	456.3	2.717	1.162	H-1→L+1 (78%), H-1→L (9%)

f_{os}= oscillator strength, H=HOMO, L=LUMO, MO=molecular orbital.

its highest absorption peak at 712.307 *nm*, due to its potent electron-withdrawing sulphonic groups in the acceptor unit, combined with a low energy value of 1.741 *eV*. The oscillator strength of 0.585 indicates that the HOMO and LUMO molecular orbitals contribute minimally, accounting for only about 4 % of the absorption. The presence of -$COOCH_3$ groups in **DTPD7** results in the minimum λ_{max}, specifically a hypochromic shift with a value of 452.530 *nm*. This shift is accompanied by the highest excitation energy of 2.740 *eV*. To enhance the maximum absorption wavelength (λ_{max}) in the designed compounds, electron-withdrawing acceptor moieties are utilized, as outlined in the Table 6. The descending order of λ_{max} values is as follows: **DTPD6** (712.307) > **DTPD5** (678.139) > **DTPD8** (667.946) > **DTPD3** (622.661) > **DTPD2** (605.806) > **DTPD4** (527.660) > **DTPD1** (527.032) > **DTPD7** (452.530) in *nm* (Table 7) The presence of effective electron-withdrawing end-capped acceptors in the compounds leads to a red-shift in the absorption spectrum, causing a change in the absorption maxima (λ_{max}) towards longer wavelengths. Additionally, the λ_{max} value for **DTPD1** is observed at 527.032 *nm*, which exceeds that of **DTPD7**. **DTPD4** has a little longer absorption wavelength at 527.660 *nm* and a higher transition energy of 2.350 *eV* compared to **DTPD1**. This change can be attributed to the addition of electron-withdrawing dichlorobenzene groups. **DTPD2** exhibits a higher absorption wavelength at 605.806 *nm* compared to **DTPD4**. This difference is attributed to the replacement of trifluoromethyl groups with benzene, as benzene being a less electron-withdrawing group compared to fluorine, might result in a relatively longer wavelength in the UV region in **DTPD2**. The higher λ_{max} value (622.661 *nm*) and lower transition energy (1.991 *eV*) observed in **DTPD3**, as compared to **DTPD2**, could potentially be attributed to the removal of cyano group as it entrapped the charges and substitution of floro groups at the terminal acceptor. The substitution of floro (-F) groups with chloro (-Cl) groups in **DTPD4**, leading to a lower absorption wavelength (527.660 *nm*) and a higher transition energy (2.350 *eV*) compared to **DTPD8**, can be attributed to the electron-withdrawing effect of the chloro group. This electron-withdrawing effect reduces resonance, resulting in a higher band gap.

The calculated λ_{max} values for the designed derivatives consistently exhibit higher values when measured in dichloromethane in contrast to the gas phase. This phenomenon is likely a consequence of solvent effects. The λ_{max} values calculated in gaseous phase for all the studied compounds fall within the range of 430-654 *nm*, which is higher than the λ_{max} value for **DTPR**, (392.194 *nm*). Among the reference and designed compounds, **DTPD5** displayed the most significant absorption peak at 654.374 *nm* and the lowest excitation energy of 1.895 *eV*. This can be ascribed to the introduction of nitro (-NO_2) groups into the thiophene ring. In solvent-phase UV-Vis absorption spectroscopy, **DTPD6** exhibits a red-shift which corresponds to the least energy gap of compound.

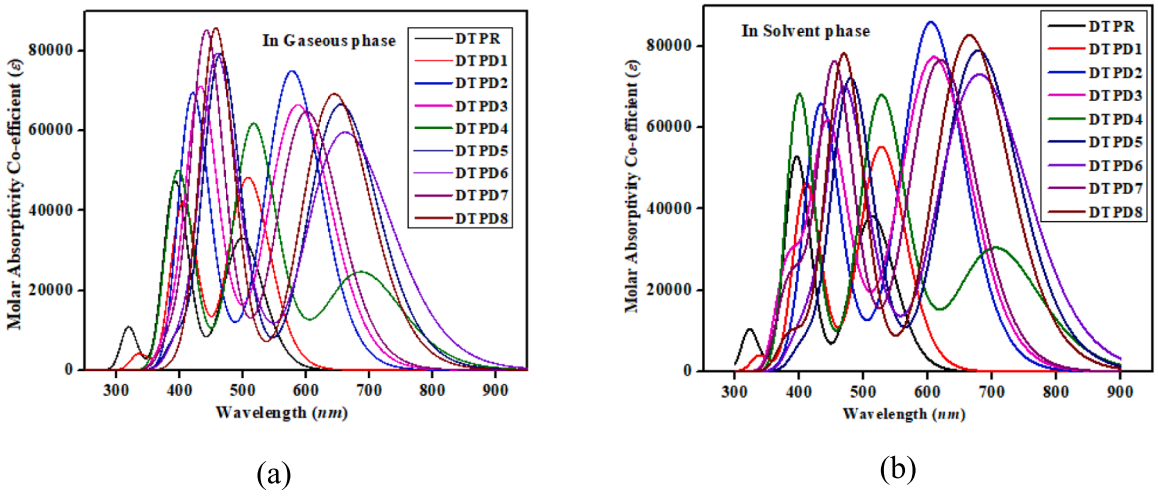

Fig. 6. Absorption spectra of **DTPR** and **DTPD1-DTPD8**: (a) in gaseous phase (b) in dichloromethane.

4. Conclusion

In current study, a series of compounds, **DTPD1-DTPD8**, were formulated by substituting the thiophene spacer unit with a selenophene unit and benzothiophene acceptors at one terminal of **DTPR**. Through quantum chemical study the effect of molecular engineering on opto-electronic properties was studied. All designed chromophores exhibited a broader absorption spectrum in the visible region with reduced E_{gap} (2.107-3.057 *eV*), and efficient charge transfer from HOMO to LUMO than that of reference chromophore. showed that all the molecules were more reactive and polarizable. The decreasing order of softness; **DTPD6 > DTPD4 > DTPD5 > DTPD8 > DTPD7 > DTPD3 > DTPD2 > DTPD1 > DTPR**. All chromophores showed significant NLO response than that of reference compound. These finding revealed that molecular engineering with selenophene placement for construction of spacer and utilization of benzothiophene acceptors for development of push-pull architecture is an easy and effective way to obtain higher *NLO* characteristics, as a consequence of the selective lower-lying lowest unoccupied molecular orbital (LUMO) with the HOMO being almost unchanged, together with the effective broadening on the absorption band. This computational work provides worthwhile insight for experimentalists to explore these attractive NLO materials for optics and electronics.

CRediT authorship contribution statement

Iqra Shafiq: Conceptualization, Methodology, Supervision. **Muhammad Khalid:** Methodology, Software, Project administration. **Ataualpa A.C. Braga:** Data curation, Formal analysis, Validation. **Zara Tariq:** Data curation, Formal analysis. **Norah Alhokbany:** Conceptualization, Methodology, Software. **Ke Chen:** Resources, Software, Supervision.

Declaration of Competing Interest

The authors declare that they have no known competing financial interests or personal relationships that could have appeared to influence the work reported in this paper.

Data availability

All data generated or analyzed during this study are included in this published article and its supplementary information files.

Acknowledgement

Dr. Muhammad Khalid gratefully acknowledges the financial support of HEC Pakistan (project no. 20-14703/NRPU/R&D/HEC/2021). A. A.C.B. acknowledges the financial support of the São Paulo Research Foundation (FAPESP) (Grants 2014/25770-6 and 2015/01491-3), the Conselho Nacional de Desenvolvimento Científico e Tecnológico (CNPq) of Brazil for academic support (Grant 309715/2017-2), and Coordenação de Aperfeiçoamento de Pessoal de Nível Superior – Brasil (CAPES) that partially supported this work (Finance Code 001). The authors extend their appreciation to the Researchers Supporting Project number (RSP2023R253), King Saud University, Riyadh, Saudi Arabia. K. C. acknowledges the support from the doctoral research fund of the Affiliated Hospital of Southwest Medical University.

Appendix A. Supplementary material

Supplementary data to this article can be found online at https://doi.org/10.1016/j.molliq.2023.123569.

References

[1] K. Lin, et al., Strong second harmonic generation in a tungsten bronze oxide by enhancing local structural distortion, J. Am. Chem. Soc. 142 (2020) 7480–7486.
[2] R. Ketavath, et al., Metal-free carbazole scaffold dyes as potential nonlinear optical phores: molecular engineering, J. Mater. Chem. C 8 (2020) 16188–16197.
[3] R. Jáuregui, J.P. Torres, On the use of structured light in nonlinear optics studies of the symmetry group of a crystal, Sci. Rep. 6 (2016) 20906.
[4] B.A. Malomed, Nonlinear optics: Symmetry breaking in laser cavities, Nat. Photonics 9 (2015) 287.
[5] M. Gullans, D.E. Chang, F.H.L. Koppens, F.G. de Abajo, M.D. Lukin, Single-photon nonlinear optics with graphene plasmons, Phys. Rev. Lett. 111 (2013), 247401.
[6] J. Jia, et al., Syntheses, third-order optical nonlinearity and DFT studies on benzoylferrocene derivatives, Dyes Pigm. 104 (2014) 137–145.
[7] D. Li, et al., Self-assembly of a series of thiocyanate complexes with high two-photon absorbing active in near-IR range and bioimaging applications, Dyes Pigm. 120 (2015) 175–183.
[8] S. Sumalekshmy, C.J. Fahrni, Metal-ion-responsive fluorescent probes for two-photon excitation microscopy, Chem. Mater. 23 (2011) 483–500.
[9] Z. Yu, et al., Photon-induced intramolecular charge transfer with the influence of D/A group and mode: optical physical properties and bio-imaging, J. Mater. Chem. C 1 (2013) 7026–7033.
[10] M. Zhang, et al., Calculated UV-Visible spectra and third-order nonlinear optical properties of heteroaromatic derivatives of stilbene inserted with 1, 3-squaraine, Synth. Met. 137 (2003) 1525–1526.
[11] N. Ma, L. Yan, W. Guan, Y. Qiu, Z. Su, Theoretical investigation on electronic structure and second-order nonlinear optical properties of novel hexamolybdate-organoimido-(car) borane hybrid, PCCP 14 (2012) 5605–5612.
[12] W. Chen, G.T. Yu, F.L. Gu, Y. Aoki, Investigation on the electronic structures and nonlinear optical properties of pristine boron nitride and boron nitride- carbon heterostructured single-wall nanotubes by the elongation method, J. Phys. Chem. C 113 (2009) 8447–8454.
[13] J. Sun, et al., New Coumarin-benzoxazole derivatives: Synthesis, photophysical and NLO properties, Dyes Pigm. 164 (2019) 287–295.
[14] H.A.R. Aliabad, M. Chahkandi, Theoretical study of crystalline network and optoelectronic properties of erlotinib hydrochloride molecule: non-covalent interactions consideration, Chem. Pap. 73 (2019) 737–746.
[15] M. Chahkandi, M. Mirzaei, Structural and particle size evolution of sol–gel-derived nanocrystalline hydroxyapatite, J IRAN CHEM SOC 14 (2017) 567–575.
[16] U. Yunus, S. Ahmed, M. Chahkandi, M.H. Bhatti, M.N. Tahir, Synthesis and theoretical studies of non–covalent interactions within a newly synthesized chiral 1, 2, 4-triazolo [3, 4-b][1, 3, 4] thiadiazine, J. Mol. Struct. 1130 (2017) 688–698.
[17] M. Chahkandi, et al., Novel cocrystal of N-phthaloyl-β-alanine with 2, 2–bipyridyl: Synthesis, computational and free radical scavenging activity studies, J. Mol. Struct. 1152 (2018) 1–10.
[18] S. Hu, et al., Growth and characterization of a chalcone derivative DMMC with strong SHG efficiency for NLO applications, Optik 231 (2021), 166410.
[19] S. Muhammad, M.R.S.A. Janjua, Z. Su, Investigation of dibenzoboroles having π-electrons: toward a new type of two-dimensional NLO molecular switch? J. Phys. Chem. C 113 (2009) 12551–12557.
[20] U. Saeed, et al., Designation and Match of Non-Fullerene Acceptors with X-Shaped Donors toward Organic Solar Cells, ChemistrySelect 4 (2019) 3654–3664.
[21] P. Judeinstein, C. Sanchez, Hybrid organic–inorganic materials: a land of multidisciplinarity, J. Mater. Chem. 6 (1996) 511–525.
[22] P.N. Prasad, B.A. Reinhardt, Is there a role for organic materials chemistry in nonlinear optics and photonics? Chem. Mater. 2 (1990) 660–669.
[23] C.C. Jiménez, et al., State of the art of boron and tin complexes in second-and third-order nonlinear optics, Inorganics 6 (2018) 131.
[24] S. Muhammad, et al., How does hybrid bridging core modification enhance the nonlinear optical properties in donor-π-acceptor configuration? A case study of dinitrophenol derivatives, J. Comput. Chem. 36 (2015) 118–128.
[25] P.G. Lacroix, I. Malfant, C. Lepetit, Second-order nonlinear optics in coordination chemistry: An open door towards multi-functional materials and molecular switches, Coord. Chem. Rev. 308 (2016) 381–394.
[26] M. Chahkandi, H.A.R. Aliabad, Crystalline network form of Gefitinib molecule stabilized by non–covalent interactions: DFT–D calculations, Chem. Phys. 525 (2019), 110418.
[27] S. Science, M. Chahkandi, A. Keivanloo Shahrestanaki, M. Mirzaei, M. Nawaz Tahir, J.T. Mague, Crystal and molecular structure of [Ni 2–H2NC (= O) C5H4N 2 (H2O) 2][Ni 2, 6-(O2C) 2C5H3N 2]· 4.67 H2O; DFT studies on hydrogen bonding energies in the crystal, Acta Crystallographica Section B Crystal Eng. Mater. 76 (2020) 591–603.
[28] Y. Patil, R. Misra, Small Molecule Based Non-Fullerene Acceptors: A Comparative Study, Chem. Rec. 18 (2018) 1350–1364.
[29] S.R. Marder, et al., Large first hyperpolarizabilities in push-pull polyenes by tuning of the bond length alternation and aromaticity, Science 263 (1994) 511–514.
[30] M. Blanchard-Desce, et al., Large quadratic hyperpolarizabilities with donor–acceptor polyenes exhibiting optimum bond length alternation: correlation between structure and hyperpolarizability, Chem.–A Eur. J. 3 (1997) 1091–1104.
[31] M. Khalid, et al., First theoretical probe for efficient enhancement of optical nonlinearity via structural modifications into phenylene based D–π–A configured molecules, RSC Adv. 12 (2022) 31192–31204.
[32] I. Khan, et al., Palladium-catalyzed synthesis of 5-(arylated) pyrimidines, their characterization, electronic communication, and non-linear optical evaluations, J. Mol. Struct. 1237 (2021), 130408.

[33] R. Canton-Vitoria, et al., Functionalization of MoS2 with 1, 2-dithiolanes: toward donor-acceptor nanohybrids for energy conversion, npj 2D Mater. Appl. 1 (2017) 13.
[34] B. Chahkandi, M. Chahkandi, An accurate DFT study within conformational survey of the d-form serine−alanine protected dipeptide, BMC Chem. 17 (2023) 138.
[35] H. Alyar, A review on nonlinear optical properties of donor-acceptor derivatives of naphthalene and azanaphthalene, Rev. Adv. Mater. Sci 34 (2013) e87.
[36] A. Mahmood, M.I. Abdullah, S.-U.-D. Khan, Enhancement of nonlinear optical (NLO) properties of indigo through modification of auxiliary donor, donor and acceptor, Spectrochimica Acta Part A: Mol. Biomol. Spectrosc. 139 (2015) 425–430.
[37] M. Chahkandi, et al., Comprehensive structural studies of molecules and crystalline networks of new ferrocene-based thiosemicarbazones, Inorg. Chem. Commun. 155 (2023), 111051.
[38] C.-H. Chen, Z.-H. Luo, I.-H. Huan, Y.-H. Chen, T.-S. Lim, Rationalize the roles of electron donating-withdrawing groups in the impacts on solvatochromism, nonlinear optics, and electroluminescence devices, Dyes Pigm. 175 (2020), 108143.
[39] H. Kang, et al., Exceptional Molecular Hyperpolarizabilities in Twisted π-Electron System Chromophores, Angewandte Chemie 117 (2005) 8136–8139.
[40] S. Aithal, P.S. Aithal, G. Bhat, Literature review on organic materials for third harmonic optical and photonic applications, Int. J. Adv. Trends Eng. Technol. (IJATET) 1 (2016) 151–162.
[41] H.A. Rahnamaye Aliabad, M. Chahkandi, Comprehensive SPHYB and B3LYP-DFT Studies of Two Types of Ferrocene: Comprehensive SPHYB and B3LYP-DFT Studies of Two Types of Ferrocene, Z. Anorg. Allg. Chem. 643 (2017) 420–431.
[42] M. Chahkandi, H.A. Rahnamaye Aliabad, Role of hydrogen bonding in establishment of a crystalline network of Cu (II) complex with hydrazone-derived ligand: optoelectronic studies, Chem. Pap. 72 (2018) 1287–1297.
[43] Z. Rahmati, M. Mirzaei, M. Chahkandi, J.T. Mague, Accurate DFT studies on crystalline network formation of a new Co (II) complex bearing 8-aminoquinoline, Inorganica Chimica Acta 473 (2018) 152–159.
[44] M. Frisch, et al., Gaussian 09, revision D. 01 (2009).
[45] Y. Zhao, D.G. Truhlar, The M06 suite of density functionals for main group thermochemistry, thermochemical kinetics, noncovalent interactions, excited states, and transition elements: two new functionals and systematic testing of four M06-class functionals and 12 other functionals, Theor. Chem. Acc. 120 (2008) 215–241.
[46] M.D. Hanwell, et al., Avogadro: an advanced semantic chemical editor, visualization, and analysis platform, J. Cheminf. 4 (2012) 1–17.
[47] C. Ravikumar, I.H. Joe, V.S. Jayakumar, Charge transfer interactions and nonlinear optical properties of push–pull chromophore benzaldehyde phenylhydrazone: a vibrational approach, Chem. Phys. Lett. 460 (2008) 552–558.
[48] M. Khalid, H.M. Lodhi, M.U. Khan, M. Imran, Structural parameter-modulated nonlinear optical amplitude of acceptor–π–D–π–donor-configured pyrene derivatives: A DFT approach, RSC Adv. 11 (2021) 14237–14250.
[49] N.M. O'boyle, A.L. Tenderholt, K.M. Langner, Cclib: a library for package-independent computational chemistry algorithms, J. Comput. Chem. 29 (2008) 839–845.
[50] V. OriginPro, OriginLab Corporation, Northamp, MA, USA, 2016.
[51] J.C. Kromann, C. Steinmann, J.H. Jensen, Improving solvation energy predictions using the SMD solvation method and semiempirical electronic structure methods, J. Chem. Phys. 149 (2018).
[52] A. Alparone, Linear and nonlinear optical properties of nucleic acid bases, Chem. Phys. 410 (2013) 90–98.
[53] A. Plaquet, et al., In silico optimization of merocyanine-spiropyran compounds as second-order nonlinear optical molecular switches, PCCP 10 (2008) 6223–6232.
[54] F. Ullah, K. Ayub, T. Mahmood, Remarkable second and third order nonlinear optical properties of organometallic C 6 Li 6–M 3 O electrides, New J. Chem. 44 (2020) 9822–9829.
[55] A. Mahmood, M. HussainTahir, A. Irfan, B. Khalid, A.G. Al-Sehemi, Computational designing of triphenylamine dyes with broad and red-shifted absorption spectra for dye-sensitized solar cells using multi-thiophene rings in π-spacer, Bull. Korean Chem. Soc. 36 (2015) 2615–2620.
[56] A. Mahmood, et al., Effect of thiophene rings on UV/visible spectra and non-linear optical (NLO) properties of triphenylamine based dyes: a quantum chemical perspective, J. Phys. Org. Chem. 28 (2015) 418–422.
[57] M. Khalid, et al., Influence of End-Capped Modifications in the Nonlinear Optical Amplitude of Nonfullerene-Based Chromophores with a D- π–A Architecture: A DFT/TDDFT Study, ACS Omega 7 (2022) 23532–23548.
[58] M.U. Khan, et al., Designing triazatruxene-based donor materials with promising photovoltaic parameters for organic solar cells, RSC Adv. 9 (2019) 26402–26418.
[59] S.S. Amiri, S. Makarem, H. Ahmar, S. Ashenagar, Theoretical studies and spectroscopic characterization of novel 4-methyl-5-((5-phenyl-1, 3, 4-oxadiazol-2-yl) thio) benzene-1, 2-diol, J. Mol. Struct. 1119 (2016) 18–24.
[60] H.P. Gümüş, Ö. Tamer, D. Avcı, Y. Atalay, Quantum chemical calculations on the geometrical, conformational, spectroscopic and nonlinear optical parameters of 5-(2-Chloroethyl)-2, 4-dichloro-6-methylpyrimidine, Spectrochimica Acta Part A: Mol. Biomol. Spectrosc. 129 (2014) 219–226.
[61] E. Inkaya, M. Dinçer, E. Şahan, İ. Yıldırım, Synthesis, spectroscopic and structural characterization of 5-benzoyl-4-phenyl-2-methylthio-1H-pyrimidine with theoretical calculations using density functional theory, Spectrochimica Acta Part A: Mol. Biomol. Spectrosc. 114 (2013) 92–100.
[62] C. James, A.A. Raj, R. Reghunathan, V.S. Jayakumar, I.H. Joe, Structural conformation and vibrational spectroscopic studies of 2, 6-bis (p-N, N-dimethyl benzylidene) cyclohexanone using density functional theory, J. Raman Spectrosc.: Int. J. Original Work all Aspects Raman Spectrosc., Including Higher Order Processes, Brillouin Rayleigh Scattering 37 (2006) 1381–1392.
[63] M. Khalid, et al., NLO potential exploration for D–π–A heterocyclic organic compounds by incorporation of various π-linkers and acceptor units, Arab. J. Chem. 14 (2021), 103295.
[64] M. Khalid, et al., Structural modulation of π-conjugated linkers in D–π–A dyes based on triphenylamine dicyanovinylene framework to explore the NLO properties, R. Soc. Open Sci. 8 (2021), 210570.
[65] W.A. Siddiqui, et al., Antibacterial metal complexes of o-sulfamoylbenzoic acid: Synthesis, characterization, and DFT study, Appl. Organomet. Chem. 36 (2022) e6464.
[66] R.G. Pearson, Absolute electronegativity and hardness correlated with molecular orbital theory, Proc. Natl. Acad. Sci. 83, 8440–8441 (1986).
[67] R.G. Parr, W. Yang, Density functional approach to the frontier-electron theory of chemical reactivity, J. Am. Chem. Soc. 106 (1984) 4049–4050.
[68] R. Parthasarathi, J. Padmanabhan, M. Elango, V. Subramanian, P.K. Chattaraj, Intermolecular reactivity through the generalized philicity concept, Chem. Phys. Lett. 394 (2004) 225–230.
[69] R.G. Parr, R.A. Donnelly, M. Levy, W.E. Palke, Electronegativity: the density functional viewpoint, J. Chem. Phys. 68 (1978) 3801–3807.
[70] R.G. Parr, R.G. Pearson, Absolute hardness: companion parameter to absolute electronegativity, J. Am. Chem. Soc. 105 (1983) 7512–7516.
[71] R.G. Parr, L.V. Szentpály, S. Liu, Electrophilicity index, J. Am. Chem. Soc. 121 (1999) 1922–1924.
[72] P. Politzer, D.G. Truhlar, Chemical applications of atomic and molecular electrostatic potentials: reactivity, structure, scattering, and energetics of organic, inorganic, and biological systems, (Springer Science & Business Media, 2013.
[73] T. Koopmans, Über die Zuordnung von Wellenfunktionen und Eigenwerten zu den einzelnen Elektronen eines Atoms, Physica 1 (1934) 104–113.
[74] J. Padmanabhan, R. Parthasarathi, V. Subramanian, P.K. Chattaraj, Electrophilicity-based charge transfer descriptor, Chem. A Eur. J. 111 (2007) 1358–1361.
[75] M. Chahkandi, Theoretical investigation of non-covalent interactions and spectroscopic properties of a new mixed-ligand Co (II) complex, J. Mol. Struct. 1111 (2016) 193–200.
[76] A. Karakas, A. Elmali, H. Unver, Linear optical transmission measurements and computational study of linear polarizabilities, first hyperpolarizabilities of a dinuclear iron (III) complex, Spectrochimica Acta Part A: Mol. Biomol. Spectrosc. 68 (2007) 567–572.
[77] M. Mirzaei, et al., Comprehensive studies of non-covalent interactions within four new Cu (II) supramolecules, CrstEngComm 14 (2012) 8468–8484.
[78] M. Khalid, et al., Efficient tuning of small acceptor chromophores with A1-π-A2-π-A1 configuration for high efficacy of organic solar cells via end group manipulation, J. Saudi Chem. Soc. 25 (2021), 101305.
[79] N. Boukabcha, et al., Synthesis, crystal structure, spectroscopic characterization and nonlinear optical properties of (Z)-N'-(2, 4-dinitrobenzylidene)-2-(quinolin-8-yloxy) acetohydrazide, J. Mol. Struct. 1194 (2019) 112–123.
[80] N. Tsutsumi, M. Morishima, W. Sakai, Nonlinear optical (NLO) polymers. 3. NLO polyimide with dipole moments aligned transverse to the imide linkage, Macromolecules 31 (1998) 7764–7769.
[81] M.N. Arshad, I. Shafiq, M. Khalid, A.M. Asiri, Exploration of the Intriguing Photovoltaic Behavior for Fused Indacenodithiophene-Based A-D–A Conjugated Systems: A DFT Model Study, ACS Omega 7 (2022) 11606–11617.
[82] A. Mahmood, A. Irfan, F. Ahmad, M.R.S.A. Janjua, Quantum chemical analysis and molecular dynamics simulations to study the impact of electron-deficient substituents on electronic behavior of small molecule acceptors, Comput. Theor. Chem. 1204 (2021), 113387.
[83] H. Eshtiagh-Hosseini, et al., Insight into the connecting roles of interaction synthons and water clusters within different transition metal coordination compounds of pyridine-2, 5-dicarboxylic acid: experimental and theoretical studies, CrstEngComm 15 (2013) 6752–6768.
[84] A.C. Serri, et al., Revisiting NLO QCD corrections to total inclusive J/ψ and ϒ photoproduction cross sections in lepton-proton collisions, Phys. Lett. B 835 (2022), 137556.
[85] S.R. Marder, et al., A unified description of linear and nonlinear polarization in organic polymethine dyes, Science 265 (1994) 632–635.
[86] M. Chahkandi, H.A.R. Aliabad, Evaluation of Non-covalent Binding Energies and Optoelectronic Properties of New CuBr 2 (C 6 H 7 N) 2 Complex: DFT Approaches, Zeitschrift anorg allge chemie 643 (2017) 180–191.
[87] H.R. Aliabad, M. Chahkandi, Optoelectronic and structural studies of a Ni (II) complex including bicyclic guanidine ligands: DFT calculations, Comput. Theor. Chem. 1122 (2017) 53–61.
[88] M.D. Zidan, M.B. Alsous, A.W. Allaf, A. Allahham, A. Al-Zier, Optical limiting action of C60 doped poly (ethylacetylenecarboxylate), Opt. Laser Technol. 44 (2012) 2282–2285.
[89] E.M. Breitung, C.-F. Shu, R.J. McMahon, Thiazole and thiophene analogues of donor- acceptor stilbenes: molecular hyperpolarizabilities and structure- property relationships, J. Am. Chem. Soc. 122 (2000) 1154–1160.
[90] M.R.S.A. Janjua, et al. A DFT study on the two-dimensional second-order nonlinear optical (NLO) response of terpyridine-substituted hexamolybdates: physical insight on 2D inorganic–organic hybrid functional materials. (2012).
[91] A. Saeed, et al., Exploring the impact of central core modifications among several push-pull configurations to enhance nonlinear optical response, J. Mol. Graph. Model. 100 (2020), 107665.

[92] S. Muhammad, et al., Benchmark study of the linear and nonlinear optical polarizabilities in proto-type NLO molecule of para-nitroaniline, J. Theor. Comput. Chem. 18 (2019) 1950030.
[93] M. Chahkandi, 51V NMR, 17O NMR, and UV–Vis computational studies of new VBPO functional models: Bromide oxidation reaction, Polyhedron 109 (2016) 92–98.
[94] M. Chahkandi, et al., Synthesis and comprehensive structural studies of a novel amide based carboxylic acid derivative: Non–covalent interactions, J. Mol. Struct. 1133 (2017) 499–509.
[95] M. Mirzaei, et al., Influence of accompanying anions on supramolecular assembly and coordination geometry in Hg II complexes with 8-aminoquinoline: experimental and theoretical studies, CrstEngComm 15 (2013) 1404–1413.
[96] M. Khalid, et al., Frontier molecular, Natural bond orbital, UV-Vis spectral stduy, Solvent influence on geometric parameters, Vibrational frequencies and solvation energies of 8-Hydroxyquinoline, Int. J. Pharm. Sci. Res 8 (2017) 13040.
[97] A. Mahmood, S.-U.-D. Khan, F. ur Rehman, Assessing the quantum mechanical level of theory for prediction of UV/Visible absorption spectra of some aminoazobenzene dyes, J. Saudi Chem. Soc. 19 (2015) 436–441.
[98] A. Mahmood, S.-U.-D. Khan, U.A. Rana, M.H. Tahir, Red shifting of absorption maxima of phenothiazine based dyes by incorporating electron-deficient thiadiazole derivatives as π-spacer, Arab. J. Chem. 12 (2019) 1447–1453.